heritage

MDPI

Article

A Tale of Two Legacies: Byzantine and Egyptian Influences in the Manufacture and Supply of Glass Tesserae under the Umayyad Caliphate (661–750 AD)

Sara Fiorentino

Department of Cultural Heritage, University of Bologna, Via Zamboni, 40126 Bologna, Italy; sara.fiorentino2@unibo.it

Abstract: The connection between Umayyad and Byzantine mosaic manufacture is a debated issue: on the one hand, Arab sources report that Umayyad caliphs received craftspeople and materials to adorn religious buildings from the Byzantine emperor; on the other hand, the reliability of these texts has long been disputed among scholars, and other possible influences have been hypothesised. Was early Islamic mosaic manufacture related to Byzantine tradition and to what extent? Were materials and artisans gathered from Byzantium and/or territories under the Byzantine control? Based on a multi-analytical approach, glass tesserae from Khirbat al-Mafjar, the Great Mosque of Damascus, and the Dome of the Rock have been analysed. Results speak of a tale of two legacies, demonstrating that, parallel to a continuity with the manufacture of glass tesserae in the late antique Levant—pointing, more specifically, to a re-use of materials from abandoned buildings—legacies other than Byzantine occurred. It emerged that Egypt definitively played a role in mosaic making during the Umayyad caliphate, acting as a supplier of skilled artisans and materials.

Keywords: ancient glass; mosaics; Islamic glass; Umayyad caliphate; Byzantine; archaeometry

Citation: Fiorentino, S. A Tale of Two Legacies: Byzantine and Egyptian Influences in the Manufacture and Supply of Glass Tesserae under the Umayyad Caliphate (661–750 AD). *Heritage* **2021**, *4*, 2810–2834. https://doi.org/10.3390/heritage4040158

Academic Editors: Nikolaos Laskaris, Georgios Mastrotheodoros, Maria Kaparou and Artemios Oikonomou

Received: 26 August 2021
Accepted: 23 September 2021
Published: 29 September 2021

1. Introduction

In 1958, upon discussing Arabs–Byzantine relations under the Umayyad caliphate, Sir Hamilton Gibb stated that they "were not confined to simple national or regional hostility, but governed by more ambivalent attitudes of both attraction and opposition" [1] (p. 223). According to him, the most perceptible legacy of the Byzantine imperial heritage was visible in the Umayyad policy of constructing magnificent religious monuments.

Arab sources reported that Umayyad caliphs requested and received from the Byzantine emperor skilled workmen and materials to construct and embellish religious buildings. In the 9th century, the historian and geographer al-Ya'qūbī alluded to the involvement of Byzantium in the construction of the Prophet's Mosque in Medina, reporting that gold, workmen, and loads of mosaics were sent to caliph al-Walīd by the Byzantine emperor [al-Ya'qūbī, Ta 'rikh, in [2] (p. 231). In the *History of Medina*, written in the 9th century by the scholar Ibn Zabāla, reference was made again to workers and mosaic cubes sent by the King of the Greeks [Ibn Zabāla, *History of Medina*, in [1] (p. 225). Al-Dinawārī (ca. 894–904 AD) reported that materials, but not craftspeople, were sent to Medina by the Byzantine emperor [2] (p. 232). Information on materials and workmen sent to Medina was also provided by the Persian explorer and geographer Ibn Rusta at the beginning of the 10th century [2] (p. 232). Mention is deserved by 10th century *Chronicle* by al-Tabarī, who reported not only that the Lord of the Greeks sent al- Walīd gold, workmen, and mosaic cubes, but also that "*[. . .] he gave orders also to search for mosaic cubes in ruined cities and sent them to al-Walid, who sent them to* [his governor in Medina] *Omar b. Abd al-Aziz [. . .]*" [al-Tabarī, *Chronicle*, in [1] (p. 232). Finally, the 10th century historian al-Maqdisī mentioned the despatch of skilful artisans and materials from the Byzantine emperor for the

construction of the Great Mosque in Damascus [al-Maqdisī, *The Best Divisions for Knowledge of the Regions*, in [2] (p.233–234).

Written sources seem, therefore, to imply that the movements of "*mosaic cubes*" and skilled artisans around the Mediterranean were not unknown under the Umayyad caliphate. However, the reliability of these sources has not been univocally recognised among scholars: should these texts be read as propaganda pieces aimed at enlightening the power of the caliphs or do they suggest that the trade between Arabs and Byzantines went on despite their rivalry [3,4]? Above all, was the Byzantine legacy the only one to influence mosaic manufacture under the Umayyad caliphate?

In 1932 the archaeologist Marguerite Gautier-van Berchem expressed her scepticism on the Byzantine "assistance" in the construction and decoration of Umayyad mosques [5] (p.156–157). Her theory was supported by the historian Jean Sauvaget, who interpreted the participation of workmen from Byzantium to the construction of the Prophet's Mosque at Medina as "*a tradition of a legendary character*" [6] (p.10–11). Discussing mosaics adorning the Dome of the Rock and the Great Mosque of Damascus, Gautier-van Berchem concluded that they had not been made by mosaicists from Byzantium, but by autochthonous artists [2]. The archaeologist referred to several ancient documents supporting her theory—the oldest was a text written by the 9th century Persian historian al-Balādhurï who spoke of the Mosque of Medina, where reference was made to "*[. . .] money, mosaics, and marble sent to him and eighty Rumī and Coptic craftsmen, inhabitant of Syria and Egypt [. . .]*" [2] (p.231); another document was the one written by the geographer al-Maqdisī, who also mentioned craftspeople from Syria and Egypt working at the Mosque of Mekka [al-Maqdisī, The Best Divisions for Knowledge of the Regions, in [2] (p. 233); finally, some official documents reported that caliph 'Abd al-Malik set aside the tax revenues of Egypt for seven years to pay for the Dome of the Rock, and the same was done by his son, caliph al-Walid, with the land tax revenues of Syria to pay for the construction and decoration of the Great Mosque in Damascus [2,7].

The Dome of the Rock in Jerusalem and the Great Mosque in Damascus are masterpieces of the Umayyad religious architecture. The Dome of the Rock was erected by caliph 'Abd al-Malik in 691 AD on the Temple Mount in Jerusalem, as reported in the inscriptions on it [8], and it is embellished with mosaics on the internal and external surfaces. The surviving original mosaics of the Dome of the Rock are located inside and, despite some conservative interventions, they still reflect the original decorative scheme [2,8–10]. There are few written references mentioning whence artisans working on the building came. The 11th century Jerusalemire preacher al-Wasiti reported that 'Abd al-Malik gathered craftsmen from all his dominions [11]. An official correspondence preserved as letters on papyrus found at Kom Ishqaw, Upper Egypt, recorded that experienced workmen sent from Egypt were employed in the construction of the al-Aqsa Mosque by caliph al-Walid [12–14]. The same document also mentioned skilled craftsmen being sent from Egypt to work on the Great Mosque in 706/7 and 709 [9,12–14]. Another letter, dated 710, referred to materials being sent to Damascus together with craftsmen [12,13].

The Great Mosque of Damascus was built between 706 and 714/5 by caliph al-Walid, entirely covered with mosaics on both the inside and the outside walls. Though large areas of the original decoration still survive on site, restorations have been made through the centuries and they are generally indicated in the inscriptions [2]. The occurrence of an Alexandrian component in the mosaics of the Great Mosque, has recently been re-examined by [15], following a theory proposed by Mab van Lohuizen-Mulder in the 1990's [16]. Detailed stylistic analysis of the Alexandrian architecture depicted in the Landscape Panorama, the largest intact area of mosaic dating to the Umayyad age, and the presence of a Nile boat with a very distinctive shape on the mosaics adorning the west arcade, would strengthen the hypothesis of an Egyptian influence in their manufacture.

Can the contribution of archaeometry help shed further light on the actual influence of more than one legacy in the manufacture of mosaics adorning Umayyad buildings? The paper aimed at providing new insights into this topic, highlighting how and to what extent

archaeometric data, framed into the current scenario of mosaic manufacturing between late antiquity and the early Islamic period, can provide a better understanding of this still debated issue.

2. Materials and Methods

An assemblage of 71 mosaic glass tesserae is discussed in this paper, comprising: 16 coloured tesserae from the qasr of Khirbat al-Mafjar, Plestine; 22 coloured and 2 colourless tesserae from the Great Mosque of Damascus, Syria; a set of 31 coloured tesserae from the Dome of the Rock in Jerusalem. All materials, with preliminary photographic and chromatic documentation, are reported in Table S1.

The tesserae from the *qasr* of Khirbat al-Mafjar (Jericho, Palestine) have been the subject of a previous preliminary study [17,18], here re-proposed within a broader research context. They belong to a larger assemblage of glass objects found in the Northern Building, erected during Hisham's caliphate (724–743) and abandoned after having been damaged by an earthquake in 748\9; consequently, the finds have been ascribed to the period between 724–748\9 [19].

The tesserae from the Great Mosque of Damascus were collected from the warehouses of the Mosque. In his report on conservative interventions carried out in the 1920s, restorer Eustache de Lorey reported having detached two fragments of the Umayyad mosaic decoration from the western portico and stored them into the warehouse [20].

The tesserae from the Dome of the Rock lack specific information on the sampling point; however, based on collected analytical data, they can be ascribed to the mosaic decoration of the Umayyad period.

The selected multi-analytical protocol encompassed: optical microscopy (OM); Natural Colour System Index chart (NCS); visible reflectance spectroscopy (VIS-RS), scanning electron microscopy coupled with an energy dispersion system (SEM-EDS); Raman microscopy (μ–Raman); X-ray powdered diffraction (XRPD); electron probe microanalysis (EPMA); laser ablation fixed with inductively coupled plasma mass spectrometry (LA–ICP–MS).

An Olympus S761 stereomicroscope (magnification up to 45X, Olympus Corporation, Shinjuku, Tokyo, Japan) associated with an Olympus Soft Imaging Solutions GMBH model SC100 camera was used for preliminary morphological inspection and documentation.

A Natural Colour System Index chart (NCS) was employed to provide a first discrimination and description of chromatic hues, both for opaque and translucent samples (http://ncscolour.com/about-us/how-the-ncs-system-works, accessed on 15 July 2021).

After preliminary NCS-aided attribution of the tesserae to chromatic macro-categories, L* a* b* numerical coordinates and the reflectance percentage for each wavelength in the visible spectrum were measured by visible reflectance spectroscopy (VIS-RS), to discriminate between different colour shades within the same chromatic macro-category. A MINOLTA CM-2600d portable spectrometer was used, equipped with an internal integrating sphere of 56-mm diameter, in reflectance geometry d/8, with three Xenon pulsed lamps, and a D65 illuminant. Calibration was performed against a $BaSO_4$ standard plate; the spectral range was 400–700 nm, with a spectral resolution of 10 nm and the area of sight of 3 mm diameter. *SpectraMagic* software (Konica Minolta, Chiyoda, Tokyo, Giappone) was employed to elaborate data; specular component excluded (SCE/0) was selected, according to [21].

For analysing micro-textural and micro-chemical features of colourants and opacifiers, scanning electron microscopy coupled with energy dispersion analysis (SEM-EDS), Raman microscopy (μ-Raman), and X-Ray powdered diffraction (XRPD) were selected. Polished sections were prepared by embedding micro-fragments of the samples in a polyester resin, which were then then polished and carbon-coated to perform the SEM investigation. Back-scattered electron signal (BSE) was used for the inspection of the morphological features of the inclusions, coupled with EDS spot measurements, to achieve a preliminary qualitative and semi-quantitative elemental analysis. Images and EDS spectra were collected on an ESEM FEI Quanta 200, equipped with an EDAX energy dispersive spectrometer (FEI

Company, Hillsboro, OR, USA). Analyses were performed in high vacuum, using an acceleration voltage of 25 kV and an energy resolution of ~200 eV at 5.9 keV; working distance was set at 10 mm, spot size was between 4 and 5 μm.

Raman spectra were collected by using a Bruker Senterra dispersive Raman spectrometer (Bruker Corporation, Billerica, MA, USA) equipped with an integrated Olympus BX40 microscope (Olympus Corporation, Shinjuku, Tokyo, Japan). A 785 nm He-Ne laser was employed, in the 300–3500 cm^{-1} region. Analytical measurements were performed with a 50× long working distance objective, operating at a power of 10 mW with a spectral resolution of 3.5 cm^{-1}. Raman measurements were performed on polished section after carbon coating removal. IRUG (Infrared and Raman Users Group) database (http://www.irug.org/, accessed on 15 July 2021) was used for the identification of the Raman bands, with papers quoted in the article as references. Being a non-destructive technique, μ-Raman was carried out as a preferential analysis on all samples under study to provide a more in-depth characterisation of colouring and opacifying phases; where spectroscopic analyses were not discriminant, XRPD was performed.

XRPD analyses were carried out on finely powdered samples manually pressed on an Ag sample holder in a Rigaku Miniflex diffractometer, employing CuKα1 radiation, in the range of 2θ: 4°–64°, θ scan speed: 1° min^{-1}; ICCD (International Centre for Diffraction Data) database was used to identify the peaks in the patterns of the analysed samples (https://www.icdd.com/, accessed on 15 July 2021).

To determine the bulk chemistry of samples, electron probe microanalysis (EPMA) was carried out on polished and carbon-coated sections. Chemical analyses of major and minor elements (Si, Ti, Al, Fe, Mn, Mg, Ca, Na, K, P, S, Cl, Cr, Co, Cu, Sn, Sb, and Pb) were performed using a CAMECA-CAMEBAX equipped with four scanning wavelength-dispersive spectrometers (WDS). A beam current of 2 nA, an acceleration voltage of 20 kV, and a spot size of 5 μm were used for Na, K, Si, and Al; for all other elements, a beam current of 20 nA, an acceleration voltage of 20 kV, and a spot size of 1 μm were used. Synthetic pure oxides were used as standards for Al, Cr, Fe, and Sn; synthetic $MnTiO_3$ for Mn and Ti; wollastonite for Si and Ca; albite for Na; periclase for Mg; PbS for Cl and Pb; orthoclase for K; apatite for P; sphalerite for S; Sb_2S for Sb; and pure elements for Co, Cu, and Ni. SMITHSONIAN GLASS A standard [22] was also employed as a reference sample. Ten points were analysed on each sample, and the mean values were calculated. The measured accuracy for the analysed elements was better than 3%. The standard deviations among the analysed points resulted to be between 1–3% and 3–5% for major and minor constituents, respectively. The detection limit for the minor elements was between 0.01 and 0.04 wt%. The correction program is based on the PAP method [23] and was used to process the results for matrix effects. EPMA data were recalculated to minimise any effect caused by elements intentionally added as colourants/decolourants and/or opacifiers, according to the procedure proposed by [24].

Laser ablation fixed with inductively coupled plasma mass spectrometry (LA–ICP–MS) was carried out to determine the concentration of 37 trace elements. Analyses were performed by a Thermo Fisher X-Series II quadrupole based ICP–MS coupled with a New Wave ablation system with a frequency quintupled (λ = 213 nm) Nd:YAG laser. Laser repetition rate and laser energy density on the sample surface were fixed at 20 Hz and ~18 J/cm^2, respectively. Analyses were carried out using a laser spot diameter of 100 μm on the same polished samples used for EPMA, after carbon coating removal. Due to the highly heterogeneous micro-structure of the tesserae, six points were analysed on each sample and the mean values were then calculated. External calibration was performed using NIST 610 and 614 glass as external standards; NIST 612 was also used as a secondary reference sample to check precision and accuracy [25]. ^{29}Si was employed as internal standard, the concentration of which was determined by EPMA following the method proposed by Longerich and colleagues [26]. The distributions of REE and the other trace elements were analysed by normalising the data to the upper continental crust [27].

3. Results and Discussion

3.1. The Base Glass

Major and minor oxides, expressed as wt% and measured by EPMA, are reported in Table S2; trace elements data, expressed as ppm, are provided in Table S3. Comparisons with standards are given in Table S4.

Analysed samples were all of a natron-type glass, with MgO and K_2O contents below 1.5 wt% (Figure 1) [28].

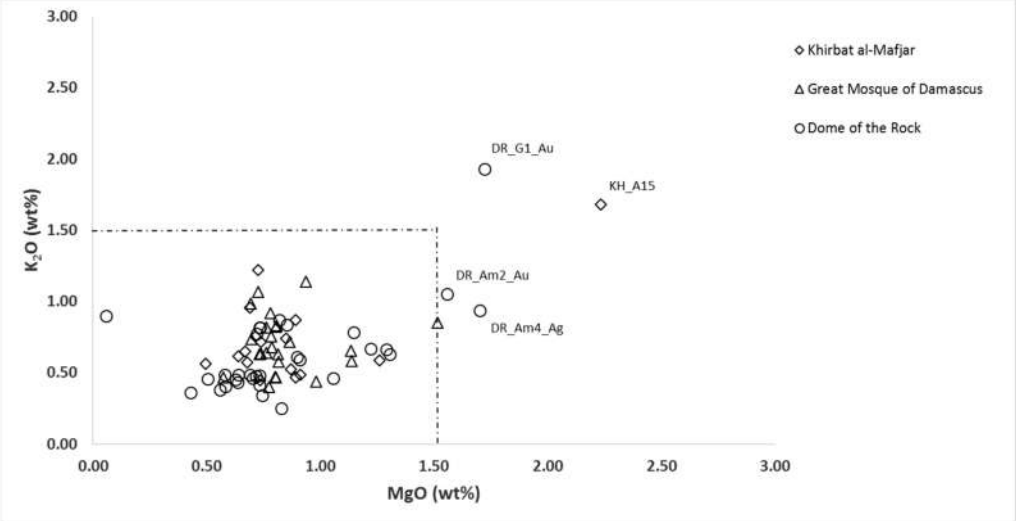

Figure 1. K_2O versus MgO bi-plot (for the opaque tesserae, reduced wt% were used).

Slightly higher MgO and K_2O contents were only detected in samples: KH_A15 (MgO = 2.23 wt%; K_2O = 1.68 wt%), DR_Am2_Au (MgO = 1.56 wt%; K_2O = 1.05 wt%), DR_Am4_Ag (MgO = 1.70 wt%; K_2O = 0.94 wt%), DR_G1_Au (MgO = 1.72 wt%; K_2O = 1.93 wt%). These values were, however, below 2.5 wt%, pointing to the use of plant ash as flux; according to the literature, they could either be linked to a contamination that occurred during the production process [29] or to the addition of plant-ash-based glass to the batch [30,31].

Based on compositional features and raw materials, analysed tesserae can be divided into the following three groups (see Table S3).

The first group, named T1, encompasses samples from: the *qasr* of Khirbat al-Mafjar (KH_R1, KH_G/V3, KH_Vsr4, KH_V5, KH_A6, KH_Vc9, KH_Ga10), the Great Mosque of Damascus (DMS_1Aa, DMS_1Ab, DMS_2Bb, DMS_10L, DMS_17R, DMS_20U), and the Dome of the Rock (DR_BK3, DR_BK4, DR_BK5, DR_G2, DR_G3, DR_G4, DR_G5, DR_G6, DR_G7, DR_GR1, DR_GY2, DR_LB1). The second group, labelled T2, comprises samples from: the *qasr* of Khirbat al-Mafjar (KH_ G2, KH_ A7, KH_ A7bis, KH_ Vc8, KH_ Am/Au11, KH_ G/V13, KH_ Am14), the Great Mosque of Damascus (DMS_2Ba, DMS_3C, DMS_5Ea, DMS_5Eb, DMS_6Fc, DMS_6Fs, DMS_8H, DMS_9I, DMS_11M, DMS_13Nv, DMS_14O, DMS_16Qa, DMS_19T), and the Dome of the Rock (DR_ A1, DR_ BK2, DR_ R1, DR_ T2, DR_ T3, DR_ T4). The third group, referred to as T3, includes samples from: the Great Mosque of Damascus (DMS_4D, DMS_7G, DMS_13Ngr, DMS_15P, DMS_18S) and the Dome of the Rock (DR_B1, DR_GY1, DR_R2, DR_T1, DR_Am1_Au, DR_Am3_Au, DR_Am4_Ag, DR_Am5_Ag, DR_Am6_Au, DR_Y1_Au).

Trace element patterns obtained by LA-ICP-MS demonstrated that different silica sources could be identified within the assemblages under study, according to the mineralogical components of the sands employed as vitrifying agent. All the tesserae belonging to group T1 showed lower strontium (Sr) and higher heavy element contents (Ti, V, Cr, Zr, Nb, Hf) compared to group T2; group T3 had higher Sr contents, comparable with T2, but higher heavy elements, analogously to T1 (Figure 2).

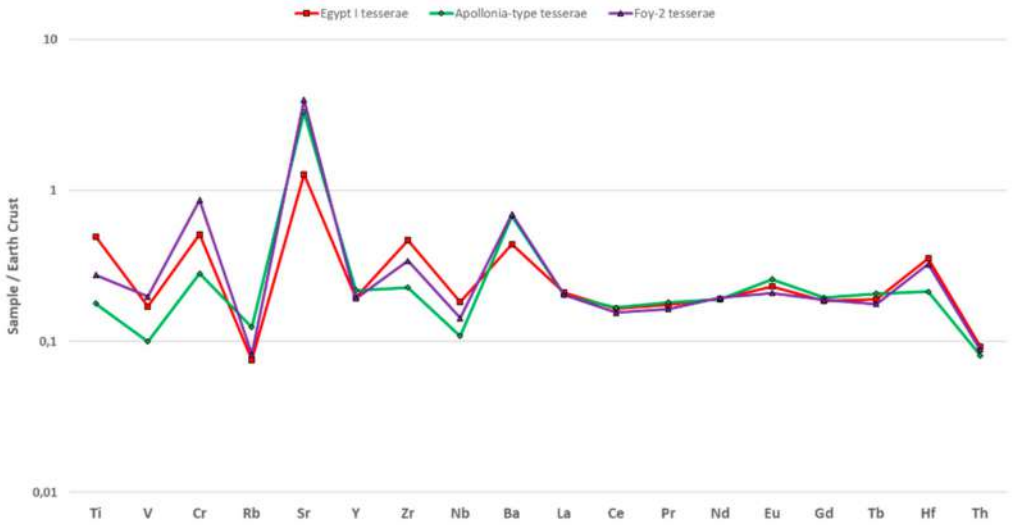

Figure 2. Comparison between trace element patterns of Egypt I (red line), Apollonia-type (green line), and Foy-2 (purple line) tesserae, obtained by LA-ICP.MS. Averages were normalised to the mean values of the continental crust [27].

Further differences among the three groups emerged when major and minor oxides were analysed, as displayed in CaO/Al_2O_3:Na_2O/SiO_2 and FeO/TiO_2:FeO/Al_2O_3 bi-plots (Figure 3a,b).

Samples belonging to group T1 had the following average contents: CaO between 2.69 and 4.34 wt%, Al_2O_3 between 2.67 and 3.79 wt%, Na_2O between 16.87 and 19.38 wt%, SiO_2 between 59.07 and 69.85wt%, TiO_2 between 0.20 and 0.35 wt%, and FeO between 0.76 and 1.79 wt%.

Data demonstrated that T1 tesserae have been made by using sands richer in the heavy accessory minerals and lower in the strontium contents; with low CaO (between 2.69 and 4.34 wt%) and high Na_2O (16.87 and 19.38 wt%), these features are consistent with Egypt I compositional category.

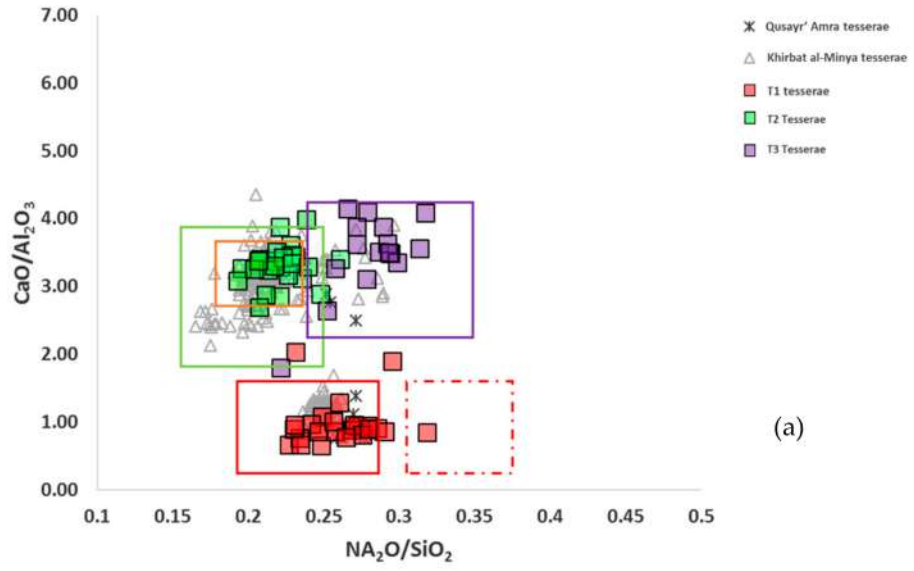

Figure 3. *Cont*.

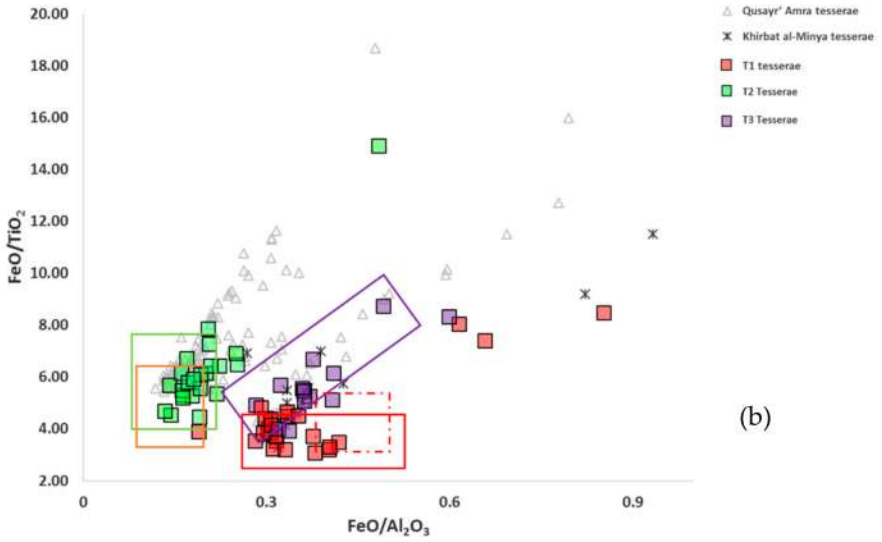

Figure 3. (**a**) CaO/Al_2O_3 versus Na_2O/SiO_2 and (**b**) FeO/TiO_2 versus FeO/Al_2O_3 bi-plot (for the opaque tesserae, reduced wt% contents were used). Green area: Apollonia-type glass [32–34], orange area: Jalame-type glass [35], red area—full line: Egypt I late antique/early Islamic glass [34,36–39], red area—dotted line: Egypt I Wadi Natrun glass [40], purple area: Foy-2 glass [38,41–44], Qusayr' Amra [45], Khirbat al-Minya [46].

Several studies have highlighted the occurrence of Egypt I glass in the late antique/early Islamic period, although named in different ways. Groups 8 and 9, identified by Foy and colleagues [37], refer to glass vessels dating to the Umayyad period (661–750): Group 8, with higher iron, aluminium, and titanium oxides contents, matches Gratuze and Barrandon's 1B group; Group 9, which might pre-date Group 8, corresponds to Gratuze and Barrandon's 1A group [36]. Egypt 1A (Group 9) and 1B (Group 8) categories were supposed to have been manufactured in the primary workshops located at Wadi Natrun (Egypt), where surveys and excavations attested primary glass furnaces datable between the 1st and the 2nd century [40,47,48]. Among glass finds excavated from 8th–9th century layers at Raya (Sinai), Kato and co-workers identified the so-called N2-a2 type, a low lime–high alumina glass comparable to Egypt I [49]. Among the late antique vessels and window glasses from Cyprus [50], few samples matching Egypt I categories were also found. Among 7th–12th centuries near eastern glassware, only two samples corresponding to Egypt I glass (named Group N4) have been identified by [34]. Lastly, recent research carried out on Islamic glass weights and stamps by [39] has distinguished three sub-categories of Egypt I glass (Egypt IA, IB, IC), each assigned to different chronological ranges between Umayyad and early Abbasid ages (ca. 697–1020).

Data in the plots highlight a separation between late antique/early Islamic Egypt I and Wadi Natrun Egypt I, where primary furnaces operating up to the 3rd century have been unearthed: late antique/early Islamic Egypt I glass has, on average, lower Na_2O, higher SiO_2, higher Al_2O_3, and slightly higher CaO than Wadi Natrun type. T1 tesserae are consistent with late/antique/early Islamic Egypt I. CaO/Sr ratios calculated for T1 tesserae are, on average, 150; as reported by Wedepohl and co-workers [51], low CaO/Sr ratios are consistent with marine carbonates, like shells (CaO/Sr = 212), while higher ratios are associated with limestone (CaO/Sr = 870). Correlation between CaO and Sr, alongside low CaO/Sr ratios, suggests the use of a coastal shell-containing sand as vitrifying agent.

Comparison between T1 tesserae trace elements patterns and the three Egypt I subgroups identified by [39] showed a clear match between T1 tesserae and Egypt IA (Figure 4), dated to the first quarter of the 8th century. These data are in line with the dating of the assemblages of tesserae under study to the Umayyad age and, more specifically, to the period when the buildings were constructed: the northern building of the *qasr* of Khirbat al-Mafjar (erected under Hisham's caliphate, between 724 and 743, and dismissed in 748/8,

following the earthquake); the Great Mosque of Damascus, constructed between 706 and 715; and the Dome of the Rock in Jerusalem, presumably started in 684/5 and completed in 691/2. Interestingly, the construction of the Dome of the Rock occurred at the end of the 7th century; this is worthy of note, as it supports the hypothesis that Egypt IA glass was in circulation under the Umayyad caliphate (661–750) prior to the 8th century [39].

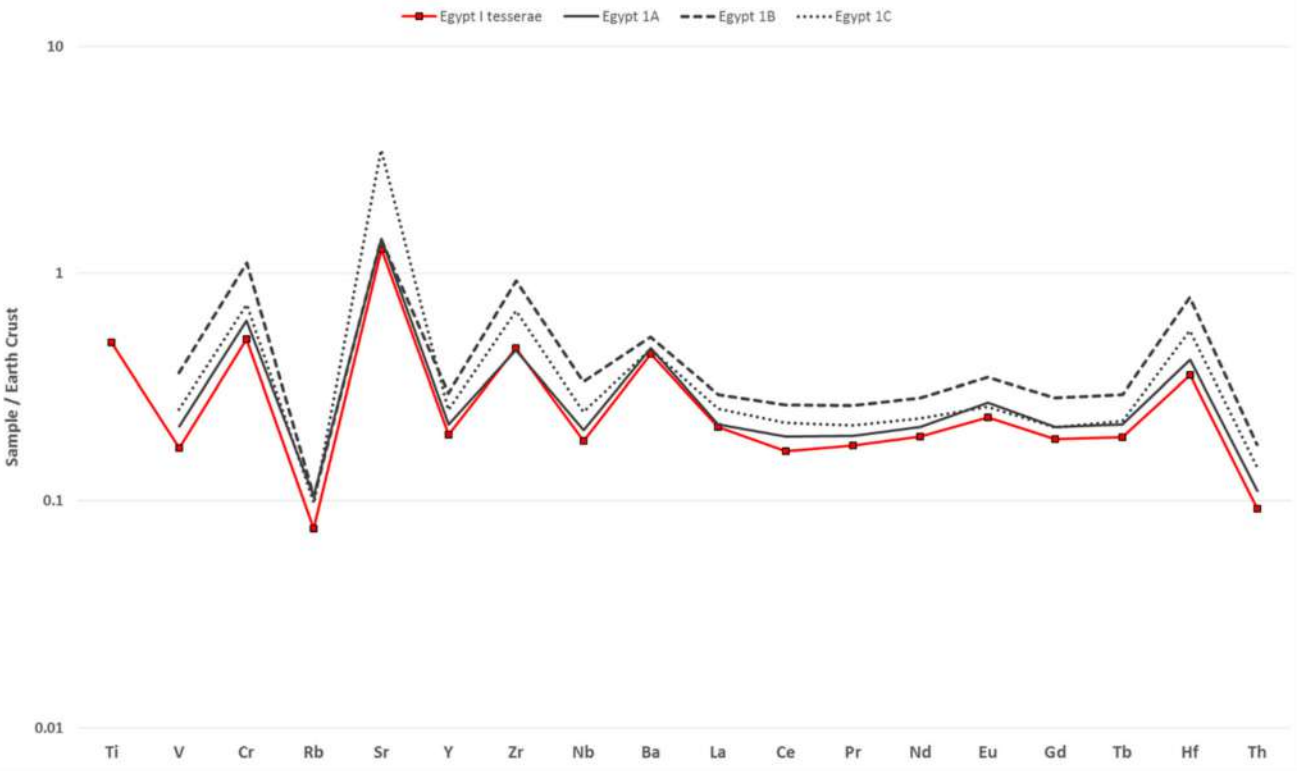

Figure 4. Comparison between trace elements pattern of Egypt I tesserae from this study and sub-groups Egypt IA, B, and C identified by [39].

Regarding the manufacture of mosaic tesserae, the use of Egypt I glass is a distinguishing feature of the Umayyad age. Apart from the *quasr* of Khirbat al-Mafjar, the Great Mosque of Damascus, and the Dome of the Rock, it has recently been found among assemblages of tesserae from the baths of Qusayr 'Amra [45] and Khirbat al-Minya [39,46].

Moving to tesserae belonging to group T2, trace element patterns showed lower heavy element contents and higher strontium (also correlated to CaO) compared to group T1 (Figure 2). This signature, in addition to the relatively high aluminium oxide content (between 2.67 and 3.79 wt%), suggests the use of a mature sand; moreover, the positive correlation between high lime and high strontium indicates a coastal sand containing shells rather than an inland one [34,52]. This was further confirmed by the low CaO/Sr ratios, with a mean value of 201.

Regarding major and minor oxides, tesserae belonging to T2 group showed: CaO between 2.69 and 4.34 wt%, Al_2O_3 between 2.67 and 3.79 wt%, Na_2O between 16.87 and 19.38 wt%, SiO_2 between 53.31 and 69.28 wt%, TiO_2 between 0.06 and 0.11 wt%, and FeO between 0.76 and 1.79 wt%. Compositional features and patterns are consistent with the use of a Levantine coastal sand, and major and minor oxides (Figure 3a,b) demonstrated that the vast majority of samples show a close match with Apollonia-type glass. Known also as Levantine I [53], this glass was produced at the primary furnaces unearthed at Apollonia-Arsuf, north Tel-Aviv; it is a soda-lime-silica glass, made by using natron as a fluxing agent. The sand source is low in oxides from heavy accessory minerals, but relatively high in alumina (>3 wt%), suggesting a mature high-silica sand with a significant feldspar content [32]. Lime is typically high (7–9 wt%), as is strontium oxide (ca. 550 ppm),

the strong correlation between them implying the use of a marine sand where lime is mainly found as shell [34,52]. Some tesserae belonging to group T2 deserve further discussion. The plots in Figure 3 show that T2 tesserae from the Great Mosque of Damascus fall at an intermediate position between Apollonia-type and Jalame-type categories. Jalame-type glass was made at the 4th century primary furnaces identified at Jalame, along the Syro-Palestinian coast and about 70–80 Km far from Apollonia [34,35]. A similar behaviour has been observed by Barford and colleagues in a study dealing with the geochemistry of Byzantine and Early Islamic glass from Jerash, in Jordan [54], leading to the hypothesis that some of the Levantine I analysed glasses could have been obtained by recycling Jalame-type into Apollonia-type. According to compositional data, it cannot be excluded that something analogous also occurred for T2 tesserae from the Great Mosque of Damascus.

T3 tesserae were characterised by: CaO between 5.26 and 9.04 wt%, Al_2O_3 between 1.76 and 3.08 wt%, Na_2O between 14.11 and 20.50 wt%, and SiO_2 between 54.35 and 68.23 wt%. These tesserae were, thus, made of a natron-based glass with slightly higher contents of magnesium (0.93–1.62 wt%), manganese (1.37–2.27 wt%), titanium (0.11 to 0.16 wt%), and iron oxides (0.58 and 1.09 wt%), with zirconium ranging from 56 to 103 ppm and strontium between 470 and 943 ppm. Outlined features are consistent with Foy-2 compositional category (Figures 2 and 3). First identified by Daniéle Foy and colleagues and believed to be of an Egyptian provenance [41], this category splits into two sub-groups: the primary production group série 2.1 and the so-called série 2.2, showing signs of recycling. While the glasses of série 2.1 have been dated to the 6th and 7th CE and seem to have been quite widespread [43,44,47,50], the recycled série 2.2 dates from 7th to late 8th CE [41]. As already noticed for a set of recently studied tesserae from the Durres amphitheatre matching Foy-2 compositional category, it is complicated to unambiguously relate samples to either of the two sub-groups [44]. Tesserae from Damascus and Jerusalem are, like those from Durres, intermediate between primary production group série 2.1 and série 2.2 (Figure 5a,b). More precisely, they are characterised by lower iron, magnesium, titanium, and zirconium contents when compared to primary production group série 2.1, and trace elements contents cannot be fully indicative as they are influenced by the addition of colourants and opacifiers to the base glass.

Lastly, a few outliers have been identified in the assemblages under study. DMS_Am/Au11 tesserae from the Great Mosque of Damascus showed compositional features more similar to the ones of Bet Eli'ezer-type glass, being characterised by higher silica (74.32 wt%), lower soda (12.09 wt%), lower lime (6.68 wt%), and higher alumina (3.17 wt%) contents. KH_Am12 translucent yellow and KH_A15 translucent light blue tesserae from Khirbat al-Mafjar, as well as DR_BK1 black and DR_G1_Au translucent green with golden leaf tesserae from the Dome of the Rock can be defined as outliers, since they showed a less definite behaviour that cannot allow unequivocally including them into the identified groups.

EPMA and LA-ICP-MS data showed that the analysed tesserae from the Great Mosque of Damascus and the Dome of the Rock match early Islamic Egypt I, Apollonia-type and Foy-2 compositional categories; differently, in the assemblage from Khirbat al-Mafjar, only early Islamic Egypt I and Apollonia-type glass groups were identified. The maps provided in Figure 6 show that glass tesserae matching Apollonia-type and Foy-2 compositional categories have mainly been recovered from sites located in the territories under the domain of Byzantium, datable back between the 5th and the 10th century, with a major amount from the 6th century.

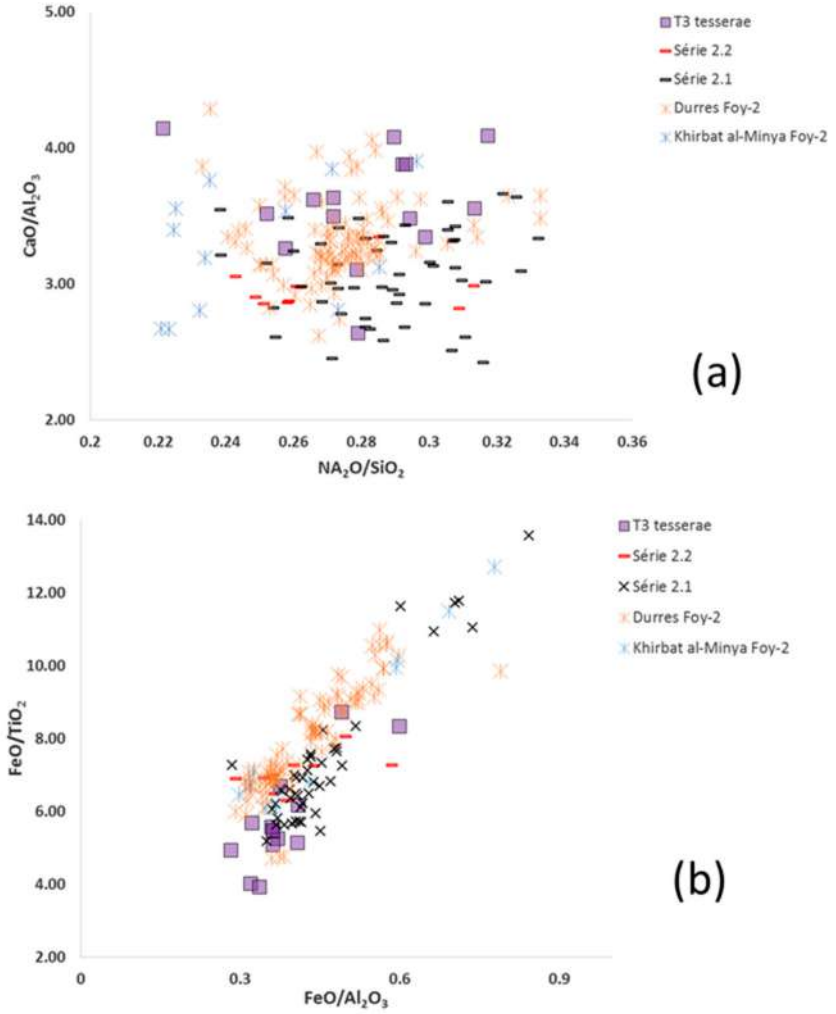

Figure 5. (**a**) CaO/Al_2O_3:Na_2O/SiO_2 and (**b**) FeO/TiO_2:FeO/Al_2O_3 bi-plots, comparing T3 tesserae with Foy-2 compositional category and related sub-groups (Foy-2.1 and Foy-2.2). Reference data from [39,41,44,46].

The detection of Apollonia-type and Foy-2 compositional categories points to continuity with the manufacture of glass tesserae in the late antique Levant. Though analyses cannot ascertain whether Umayyad Apollonia-type and Foy-2 tesserae were freshly made or gathered from ruined and dismantled pre-existing monuments, further inferences can be drawn by taking into consideration data from recent studies on early Islamic glass vessels. Research undertaken by Phelps and colleagues [34] demonstrated a high variability of glass typologies and recipe changes in the Umayyad age (661–750). Two noteworthy pieces of information have to be considered here: the absence of Foy-2 compositional category, both in the 7th and in the 8th century, and the decrease of Apollonia-type glass in the first half of the 8th century. As, contrariwise, Foy-2 and Apollonia-type glass are recurrent in Umayyad assemblages of mosaic tesserae, this fact could support the hypothesis of tesserae recovered from dismantled sites, previously adorned with mosaics, rather than freshly made.

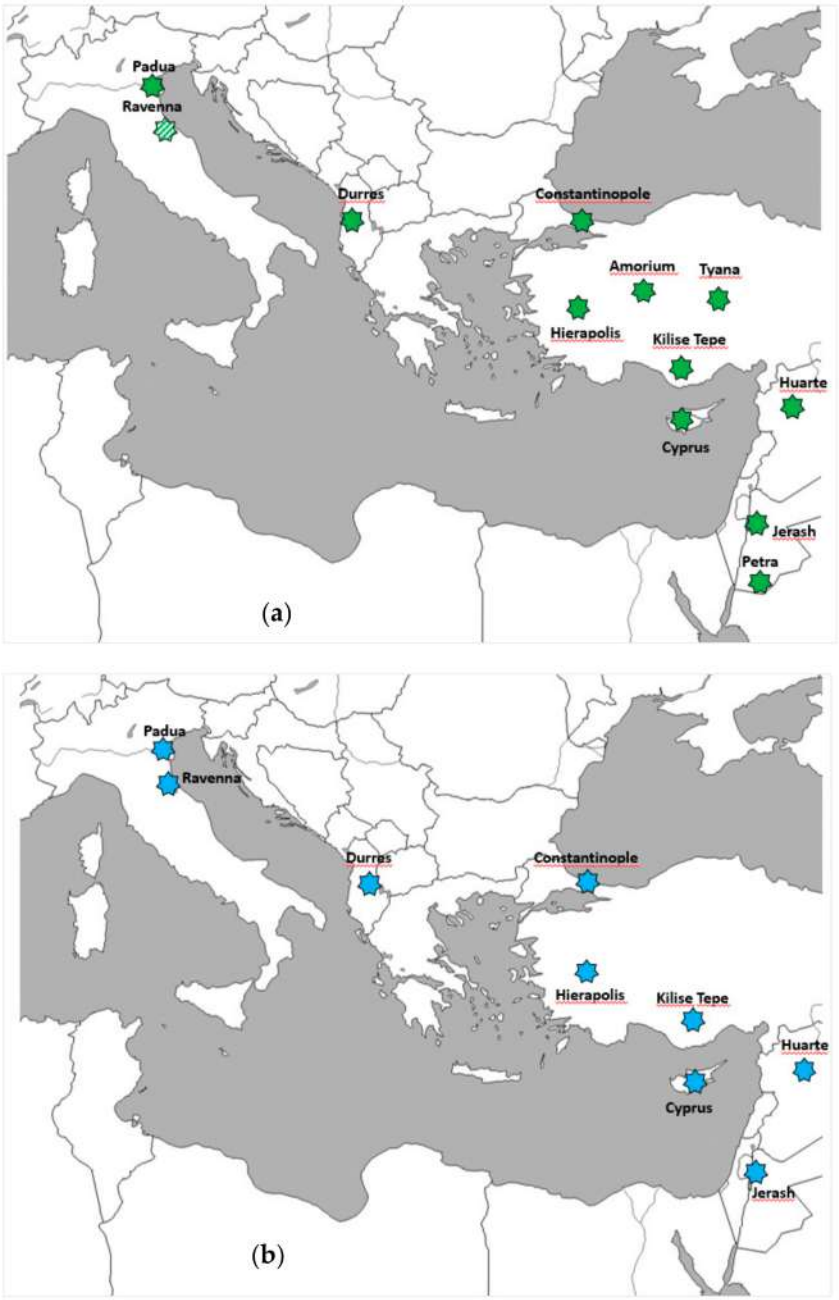

Figure 6. Distributional maps of sites across the Mediterranean basin where (**a**) Apollonia-type/Levantine I and (**b**) Foy-2 tesserae have been found. References: Padua, 6th century [55,56]; Ravenna, 6th century [57–63]—site tag is filled in a different way because, in the references, the base glass is generically termed *Levantine* rather than *Levantine I*; Durres, 6th–8th century [44]; Constantinopole, 6th century [64]; Hierapolis, 6th century [43]; Amorium, 10th century [65]; Tyana, 5th century [66]; Kilise Tepe, 5th–6th century [43]; Huarte, 5th century [67]; Cyprus, 6th century [38]; Petra, 5th–6th century [68,69]; Jerash, 4th–8th century [70].

The key feature that distinguishes Umayyad mosaic tesserae assemblages from any other is the occurrence of Egypt I compositional category, found in all the assemblages under study. This finding is a tangible proof of legacies other than Levantine in the manufacture of Umayyad mosaics. According to the literature, Apollonia-type, Egypt I, and Foy-2 compositional categories have been detected among all analysed assemblages of glass tesserae datable back to the Umayyad caliphate in the Near East (661–750): the baths of Qusayr' Amra, Jordan [45]; the residential complex at Khirbat al-Minya, Israel [46];

the *qasr* of Khirbat al-Mafjar, Palestine [17,18]; the Great Mosque of Damascus, Syria; and the Dome of the Rock, Israel. Despite their significance, data on the base glass are not sufficient to outline a complete scenario, as another issue needs to be considered: were tesserae transported as an already finished product, or were they delivered as raw glass to be locally coloured and opacified?

3.2. Colouring and Opacifying Agents

To evaluate possible answers to the above question, an in-depth characterisation of colourants and opacifiers is mandatory.

As it has been discussed more in-depth elsewhere [57,71,72], the exact classification of the colours of glass tesserae on an entirely objective basis stands as the first issue to be addressed, to avoid any subjective description and to provide a reliable criterion for the selection of tesserae to be analysed and, at a later stage, compared.

Figure 7 provides an overview of NCS-Red tesserae (KH_R1, DR_R1, DR_R2). Reflectance curves show an increase of intensity for the wavelengths above 580 nm, the red region of the visible spectrum (Figure 7a). SEM-BSE images highlight a heterogeneous micro-structure, dotted with nanometric droplets of copper—as demonstrated by EDS analyses (Figure 7b–d). XRPD exactly characterised crystalline phases as metallic copper, responsible for the red hue as well as for the opacity (Figure 7e). Features of opaque red tesserae are consistent with so-called "dullish red" glass, a low-lead (PbO 1–2 wt%), low-copper (CuO about 2–3 wt%) glass with nanometric rounded particles of metallic copper dispersed into the matrix [71,73–76].

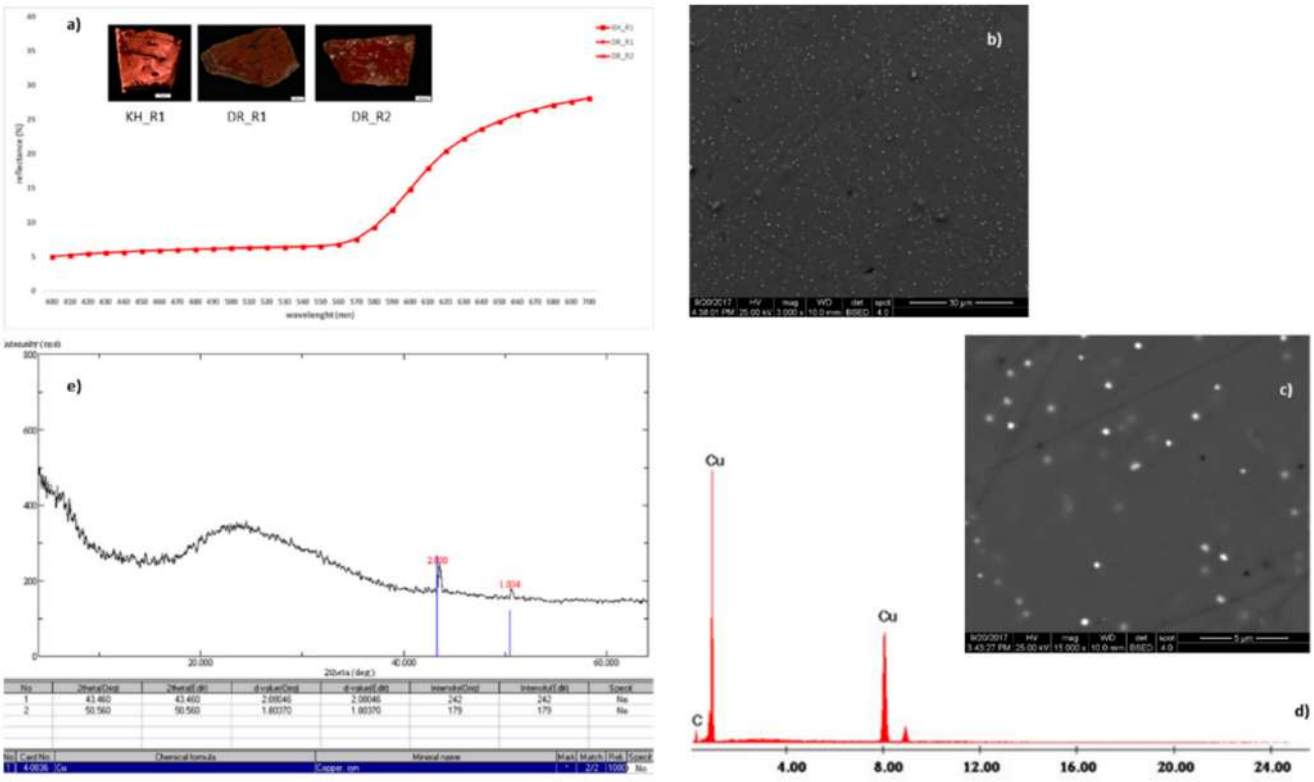

Figure 7. NCS-Red tesserae: (**a**) VIS-RS curves; (**b**,**c**) BSE images of tessera DR_R2, showing the micro-textures of the vitreous matrix, dotted with regularly distributed nanometric rounded particles; (**d**) EDS spectrum acquired on one of the rounded particles; (**e**) X-ray diffraction pattern of tessera DR_R2.

Figure 8 displays NCS-Black tesserae (DMS_13Ngr, DR_BK1, DR_BK2, DR_BK3, DR_BK4, DR_BK5). All samples showed an entirely flat behaviour in the wavelength range 400–700 nm, consistent with the absorption of all the visible radiation responsible for the black-looking colour (Figure 8a). The tesserae were made of opaque dark red stripes

alternated with translucent green ones (Figure 8b). SEM-BSE images highlighted different atomic number average between the green (lower atomic number) and the red (higher atomic number) bands, where nanometric droplets could be observed (Figure 8c–e). EDS measurements (Figure 8f,g) showed that, in the red stripes, a relatively higher copper content was found compared to green ones, and the iron content was higher as well (CuO stripes: 0.29–3.37 wt%; CuO matrix: 0.24–3.50 wt%; FeO stripes: 0.93–4.21 wt%; FeO matrix: 0.75–3.54 wt%). Green/red banded tesserae are not unattested in the literature: in Roman mosaics from Pordenone, Trento and Aquileia [73,77], several green/red-banded and orange/red-banded tesserae were found, all coloured by the addition of copper-based phases. It is, however, still unclear whether the bi-coloured pattern could always be interpreted as an accidental occurrence (like a failed attempt to produce red glass) or if a deliberate combination of two different kinds of glass took place [71].

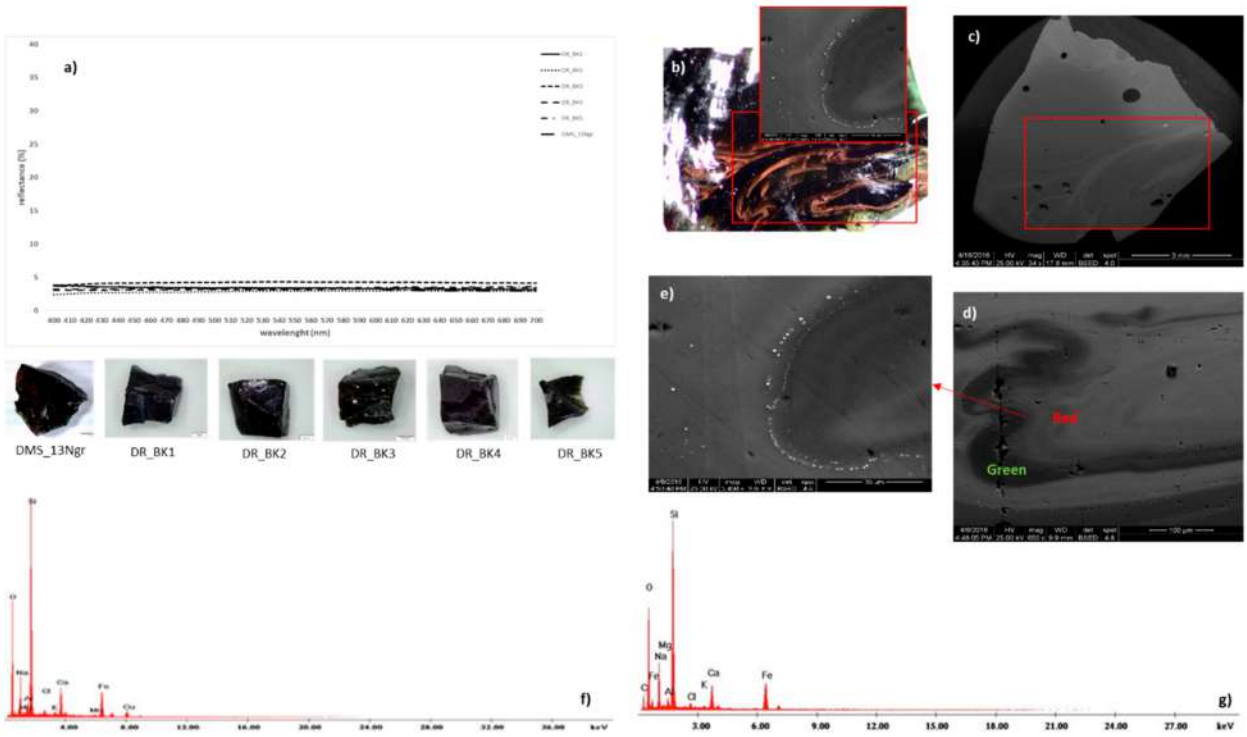

Figure 8. NCS-Black tesserae: (**a**) VIS-RS curves; (**b**) OM image of tessera DMS_13Ngr; (**c**,**d**) BSE images showing non-homogenous, zoned vitreous matrix; (**e**) BSE detail of the area where green and red glass were juxtaposed (note the nanometric rounded particles); (**f**,**g**) EDS spectra acquired on red and green stripes of glass. This figure has been re-adapted by [71].

In Figures 9 and 10, colouring and opacifying agents found in NCS-Blue tesserae (KH_A7, KH_A7bis, KH_A15, DMS_4D, DMS_10L, DR_LB1, DR_T1, DR_T2, DR_T3, DR_T4) are summarised. The reflectance curves had different profiles (Figure 9a): while some (DR_T1, DR_T2 and DR_T3) showed well-defined bell-shapes with a reflectance peak between 440 and 540 nm (the blue and the green zones of the visible spectrum), others (DR_LB1, DMS_10L and KH_A7) had a less pronounced bell shaped-outline, with variations in the reflectance percentages. Figure 9b explains how the different profiles of the curves and the percentages of reflectance can be related to the contents of copper oxide in the matrix, responsible for the light blue chromatic shades, as well as to the presence of PbO, enhancing the brilliance of the tesserae and, therefore, resulting in higher lightness (Figure 9c). The dark blue tessera DR_B1 showed a completely different reflectance curve, consistent with those reported in the literature for tesserae coloured by the addition of cobalt [78,79].

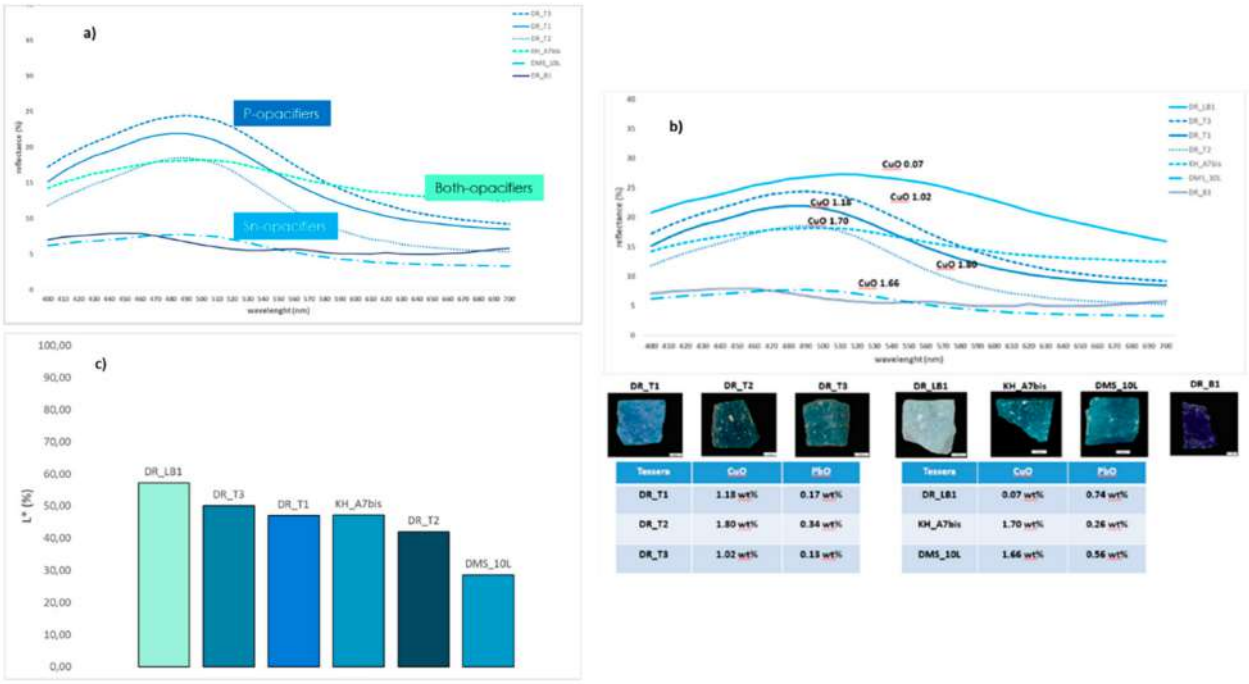

Tessera	CuO	PbO
DR_T1	1.18 wt%	0.17 wt%
DR_T2	1.80 wt%	0.34 wt%
DR_T3	1.02 wt%	0.13 wt%

Tessera	CuO	PbO
DR_LB1	0.07 wt%	0.74 wt%
KH_A7bis	1.70 wt%	0.26 wt%
DMS_10L	1.66 wt%	0.56 wt%

Figure 9. NCS-Blue tesserae: (**a**) comparison between reflectance curves acquired by VIS-RS; (**b**) CuO and PbO wt% contents—measured by EPMA—related to the reflectance curves, to indicate possible correlation between the differently shaped profiles of the curves and, on the one hand, the contents of CuO, responsible for the light blue chromatic shades, on the other hand, the presence of PbO, enhancing the brilliance of the tesserae; (**c**) Luminosity (L*) percentages measured by VIS-RS. Note how L* values were higher in tesserae where higher PbO wt% contents have been found.

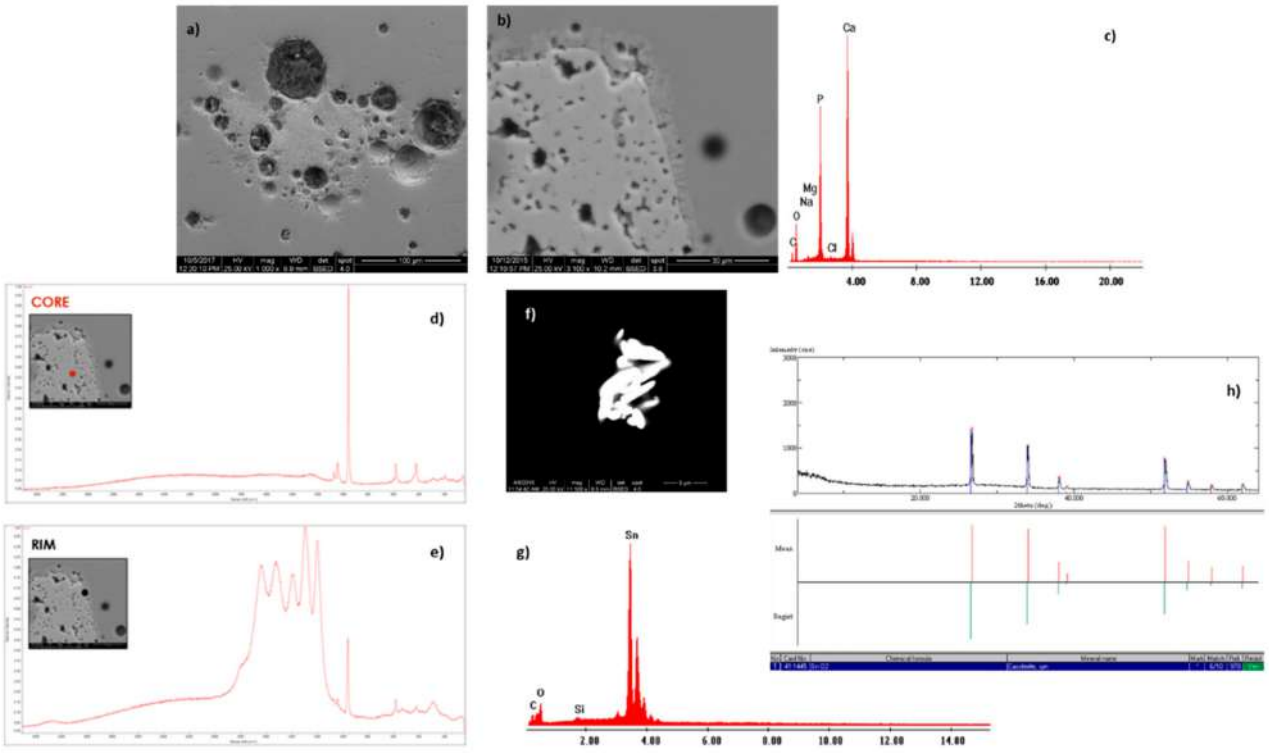

Figure 10. NCS-Blue tesserae: (**a**,**b**) SEM-BSE images of P-based inclusions, without and with reaction rim (tesserae DR_T3 and KH_A7bis); (**c**) EDS spectrum acquired on the core of the inclusion; (**d**,**e**) µRaman spectra acquired on P-based inclusions with rims found in tessera KH_A7bis; (**f**,**g**) SEM-BSE image and EDS spectrum of Sn-based crystals found in tessera DMS_10L; (**h**) X-ray diffraction pattern of tessera DMS_10L.

A combined SEM-EDS and micro-Raman approach allowed an in-depth analysis of the micro-structures of the tesserae belonging to NCS-Blue category, and the results demonstrated that they were all (but DMS_10L and DR_B1) opacified with powdered bone ash. BSE images highlight a non-homogeneous matrix, with gas bubbles and inclusions of irregular shape, whose dimensions ranged from about 60 μm up to millimetres (Figure 10a,b). Inclusions bigger than 100 μm showed a reaction rim darker than the core, while smaller inclusions did not have rims and were more compact. Despite their conformation, EDS spectra showed that the inclusions were mainly made of calcium and phosphorus (Figure 10c). Micro-Raman measurements (Figure 10d,e) demonstrated that the cores of the inclusions were made of hydroxyapatite, with bands located in the region from 400 to 1100 cm^{-1} [80,81]. Raman spectra acquired on the rims proved that they were consistent with β-rhenanite (β-NaCaPO4), a crystalline phase whose precipitation in the glass as been observed at around 650 °C [80,82]. Smaller calcium phosphate inclusions (<100 μm) did not have reaction rims, and Raman spectra acquired on them were highly comparable to those of the cores of the larger grains; it is, therefore, likely that the modification of hydroxyapatite into β-rhenanite was not completed in crystals having smaller dimensions. DMS_10L and DR_B1 were the only NCS-Blue tesserae where, instead of calcium phosphate, SnO_2 crystals were detected (Figure 10f–h). Interestingly, the reflectance curve of tessera DMS_10L had a different shape compared to those opacified with P-based inclusions; its feature resembled the reflectance curve of KH_A7bis, where micrometric inclusions of cassiterite have been detected in the matrix, with calcium phosphate as well. The main difference between the curves of tesserae DMS_10L and KH_A7bis is was to the reflectance percentage, which was higher in KH_A7bis; it cannot be excluded that the choice of one or the other opacifying agent could have been linked to the necessity of obtaining more or less saturated (and, thus, brilliant) hues. In all the light blue tesserae, the presence of copper dispersed into the glassy matrix and acting as main colouring agent was detected (EMPA data performed on the glassy matrix showed CuO ranging from 1.70 to 2.42 wt%); cobalt was only found in the dark blue tessera DMS_4D (CoO = 0.08 wt%).

In Figure 11 NCS-Yellow tesserae (KH_G2, KH_GV3, DMS_7G, DMS_9I, DMS_28b, DR_GY1, DR_GY2) are shown. Reflectance curves all had an increase in reflectance from about 530 nm, consistent with the yellow part of the visible spectrum (Figure 11a) SEM-BSE inspection highlighted strongly heterogeneous micro-structures of the matrices, with brighter bands of a higher average atomic number (Figure 11b,c). Micrometric crystals with either anhedral or subhedral habitus have been detected, mainly in the bands (Figure 11d), and EDS spot measurements demonstrated that the crystals were mainly made of lead and tin (Figure 11e). The micro-Raman spectra acquired on the crystals (Figure 11f) showed bands at 68, 138, 327, and 455 cm^{-1}, consistent with lead–tin yellow type II [83–85], a cubic-structured lead–tin silicon oxide that can show different stoichiometries [either $PbSnO_3$, $Pb(Sn, Si)O_3$, or $PbSn_2SiO_3$]. Comparison between the Raman spectra of pure $PbSnO_3$ and $PbSn_{1-x}Si_xO_3$ was unfeasible, as a signature of $PbSnO_3$ alone is not reported in the literature. As discussed elsewhere [71,72], a more exact identification of the mineralogical phases can be achieved through XRPD, as patterns seem to compare best to $PbSnO_3$. It is also interesting to note that reflectance curves of NCS-Yellow tesserae closely match those reported by Cloutis and colleagues [86] for powdered lead–tin-oxide-based yellow pigments; more precisely, the closest similarity occurs with standard PIG818, a lead–tin yellow type II.

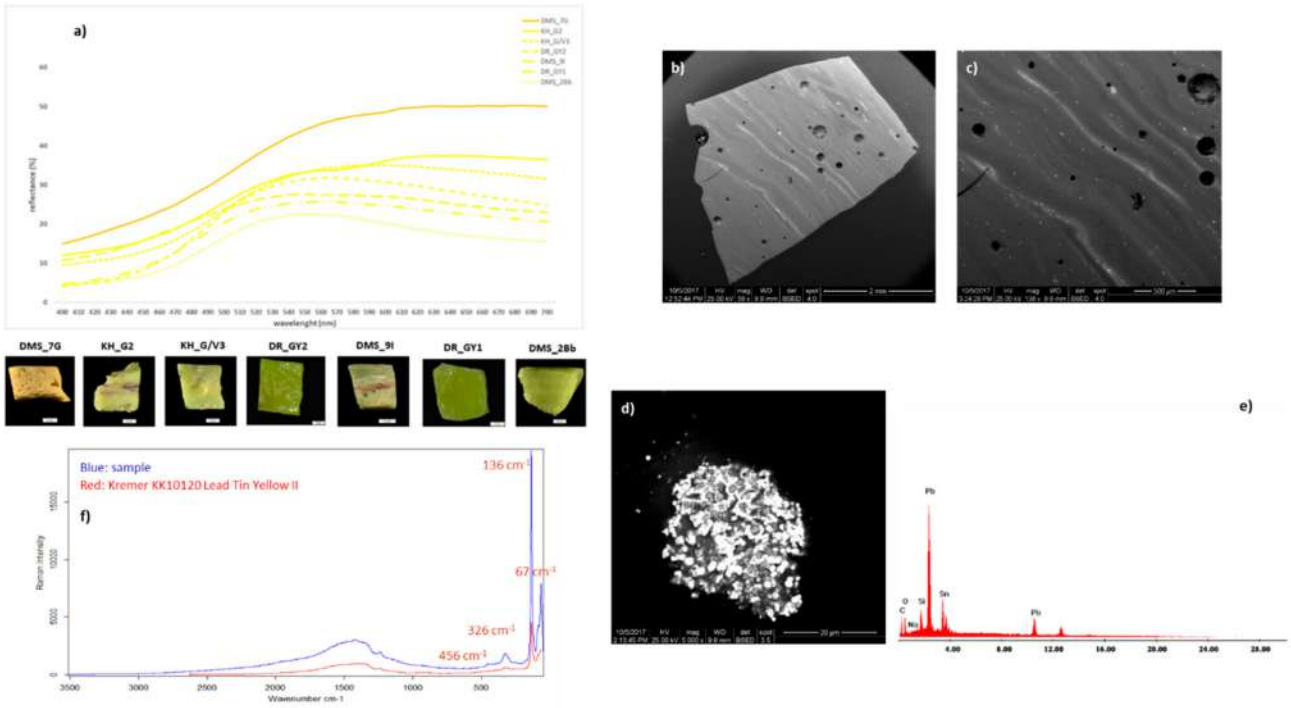

Figure 11. NCS-Yellow tesserae: (**a**) VIS-RS curves; (**b**–**d**) SEM-BSE images showing micro-textural features of tessera DR_GY1, with details of stripes and clusters of subhedral crystals; (**e**) EDS spectrum acquired on the subhedral inclusions; (**f**) μRaman spectra acquired on the subhedral crystals.

In NCS-Green tesserae, a variety of colouring and opacifying agents have been detected: tesserae KH_Vsr4, KH_V5, KH_Vc8, KH_Vc9, DMS_1Aa, DMS_1Ab, DMS_3C, DR_G2, DR_G3, DR_G4, DR_G5, DR_G6, and DR_G7 have been coloured and opacified with lead–tin yellow type II and copper; in tesserae KH_A6, KH_Ga10, DMS_5Ea, DMS_16Qa, and DR_Gr1 calcium phosphate and copper were found; and tesserae DMS_5Eb, DMS_17R, DMS_20U, and DR_A1 showed the presence of cassiterite and copper. Figure 12 provides reflectance curves of tesserae belonging to the NCS-Green category: differences were observed in terms of both reflectance intensity and profiles of the curves, linkable to the different shades of green encountered inside the green macro-category and ascribable to the compositional features of the tesserae. Reflectance curves of NCS-Green tesserae, whose colour shades and opacity degrees are ascribable to the addition of lead–tin yellow type II and copper are displayed in Figure 12a, while in Figure 12b NCS-Green tesserae opacified with cassiterite and coloured by copper are shown. The profiles of the curves in Figure 12a looked like a combination between those of a copper-coloured light blue tessera and a lead–tin yellow type II-coloured yellow one: a peak occurred between 480 and 560 nm, followed by a reflectance decrease above 550 nm. Conversely, the profiles of the curves displayed in Figure 12b more closely resembled those of NCS-BLUE tesserae coloured by copper. Moreover, NCS-Green tesserae whose colour shades were more turned towards a yellowish-green (KH_Vsr4, DMS_3C, DR_G2, DR_G4, DR_G7) showed trends of the reflectance curves more similar to those of the yellow tesserae (Figure 12a), while NCS-Green tesserae whose colour shades were more turned towards a green hue showed reflectance curves more similar to those of the blue tesserae coloured by the addition of copper. In the case of NCS-Green tesserae opacified and coloured by lead–tin yellow type II and copper, no correlation was found between copper contents and reflectance—a decrease of reflectance was not always observed when copper contents increased. The lead and tin oxides contents did not seem to impact on the reflectance either (Figure 12c).

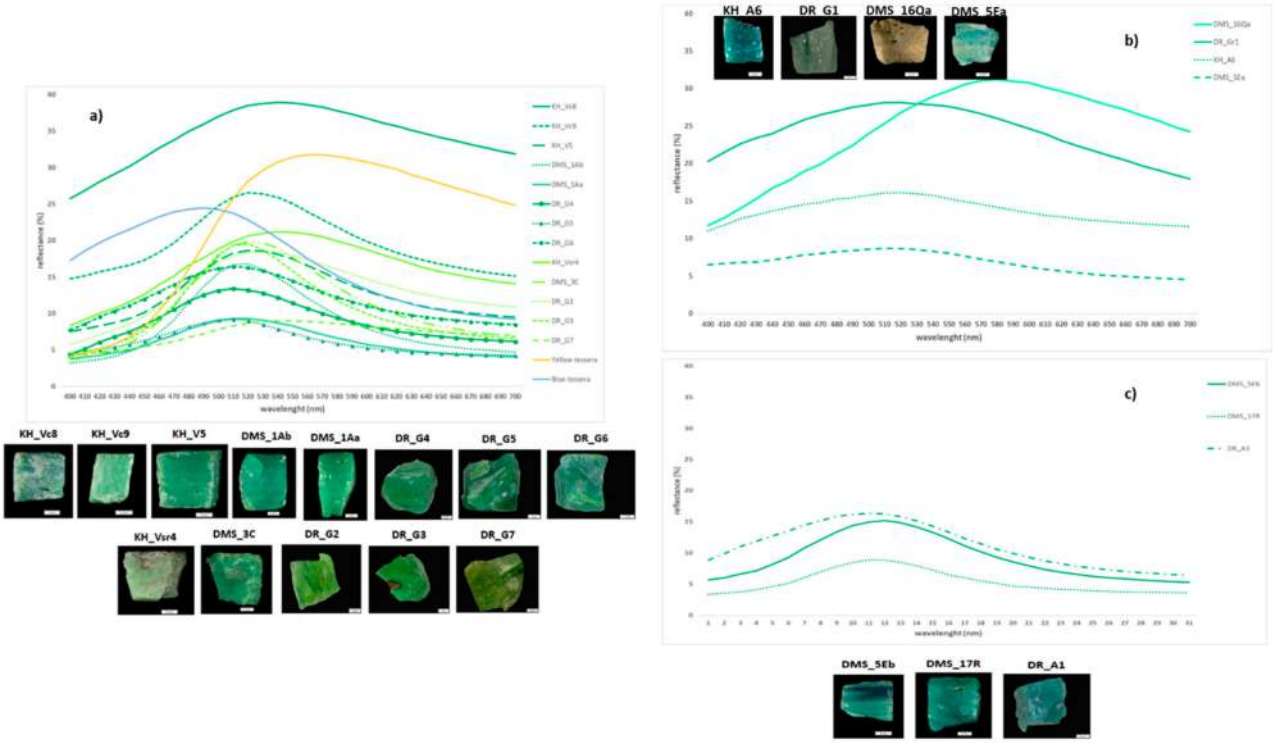

Figure 12. NCS-Green tesserae: (**a**) VIS-RS curves of green tesserae where lead–tin yellow type II and copper have been detected; (**b**) VIS-RS curves of green tesserae with calcium phosphate and copper; (**c**) VIS-RS curves of green tesserae containing cassiterite and copper.

Further considerations on opaque green tesserae with calcium phosphate and copper (KH_A6, DMS_5Ea, DMS_16Qa and DR_Gr1) are needed. These samples showed reflectance curves resembling those recorded for NCS-Blue tesserae, with peaks between 440 and 540 nm (Figure 9); a slightly different profile was observed for tessera DMS_16Qa, with a higher reflectance percentage compared to other yellow tesserae and a shifted peak, occurring at about 570–580 nm (Figure 12b). Detected differences can be linked to compositional features, as 16Qa tessera was characterised by a PbO content of 2.33 wt%. The higher reflectance percentage can, thus, be attributed to the addition of lead oxide to the base glass, responsible for an increase in the brilliance and, therefore, reflectance of the surface.

Figure 13 provides an overview on NCS-Green tesserae coloured and opacified with lead–tin-based phases plus copper (green tesserae containing calcium phosphates or cassiterite will not be discussed further as no micro-textural and/or micro-compositional differences were detected against blue tesserae with the same micro-chemistry). Though the use of lead–tin yellow type II has been detected in both yellow and green tesserae, accurate study of the micro-textures highlighted some differences. The yellow tesserae showed a higher abundance of subhedral crystals in the glassy matrices, mainly found as aggregates; in the green-shaded tesserae, a higher distribution of acicular-shaped crystals, whose composition was consistent with SnO_2, was observed, while subhedral inclusions were more sporadic and often found isolated (Figure 13a–g). As the persistence of cubic lead stannate (responsible for the yellow colour) is mainly dependent upon temperature [87,88], it can be hypothesised that different firing temperatures were used to achieve the different chromatic shades: lead–tin oxide type II crystals are, in fact, stable at up to temperatures between 750 °C and 1000 °C; at higher values, crystals begin to decompose and re-crystallise as SnO_2. Therefore, it is likely that the green tesserae were produced at higher furnace temperatures than yellow, as they showed a relatively high abundance of SnO_2 crystals in the glassy matrix.

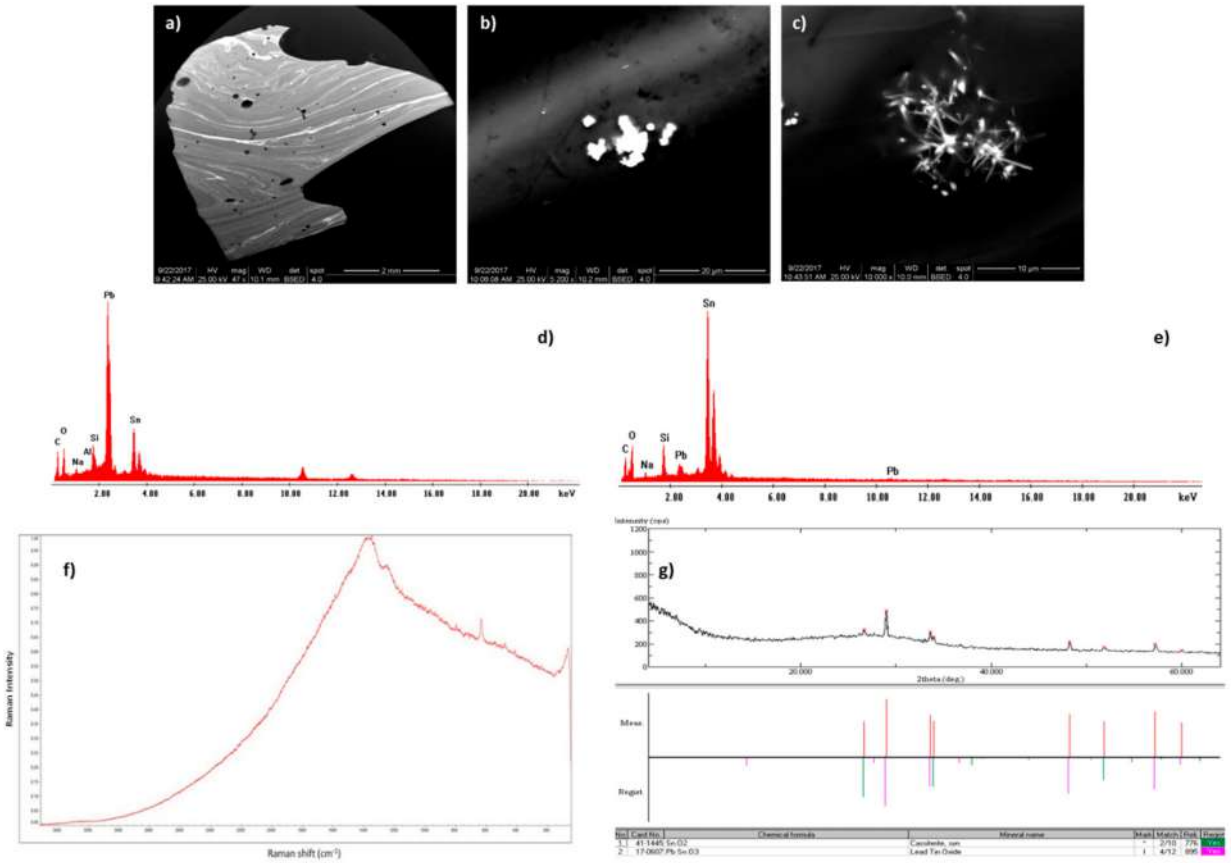

Figure 13. NCS-Green tesserae: (**a**–**c**) SEM-BSE images showing micro-textural features of tessera DR_G5, with details of stripes and clusters of subhedral and acicular crystals; (**d**,**e**) EDS spectra acquired on subhedral and acicular inclusions; (**f**) μRaman spectra acquired on the acicular crystals; (**g**) X-ray diffraction pattern of tessera DR_G5, showing the occurrence of both $PbSnO_3$ and SnO_2.

A short note on the translucent and transparent tesserae found among the three assemblages of analysed samples. KH_Am/Au11 and KH_Am14 translucent yellow tesserae showed relatively high MnO contents of 1.87 and 2.58 wt%, indicating its addition as a colouring agent. The translucent yellow tesserae KH_G/V13 and KH_Am12 showed neither higher MnO contents, nor any other metal oxides whose contents could suggest a deliberate addition to the glass. The translucent blue tessera DMS_4D was coloured by the addition of CoO (0.08 wt%). DMS_6Fs, DMS_18S, and DMS_19T translucent yellow tesserae, respectively, had MnO contents of 4.04, 0.89, and 2.55 wt%, indicating an intentional addition as colouring agent. DMS_6Fc and DMS_15P colourless tesserae showed relatively high MnO contents as well, respectively being 5.21 and 1.71 wt%, here acting as a decolourant. All the translucent yellow tesserae from the Dome of the Rock (DR_Am1-Au, DR _Am2_Au, DR_Am3_Au, DR_Am4_Ag, DR_Am5_Ag, DR_Am6_Au, and DR_Y1_Au) had MnO contents ranging between 1.62 and 2.43 wt%, responsible for the colour; the translucent green tessera DR_G1_Au showed a CuO of 1.16 wt, acting as colouring agent.

The colouring and opacifying agents found in the Umayyad assemblages under study do not represent a novelty in the panorama of the materials used in the manufacture of mosaic glass tesserae. Figure 14 shows the distributional maps of the assemblages in which lead–tin-based and phosphorus-based inclusions have been detected. Based on the literature, it can be observed that the use of bone ash was not attested before the 5th century; moreover, the majority of assemblages came from archaeological sites located in the eastern Mediterranean basin. Analogously, most of the sites where tesserae containing tin- and lead–tin-based compounds have been found are located in the eastern area of the Mediterranean basin and can be dated between the 6th and the 8th century.

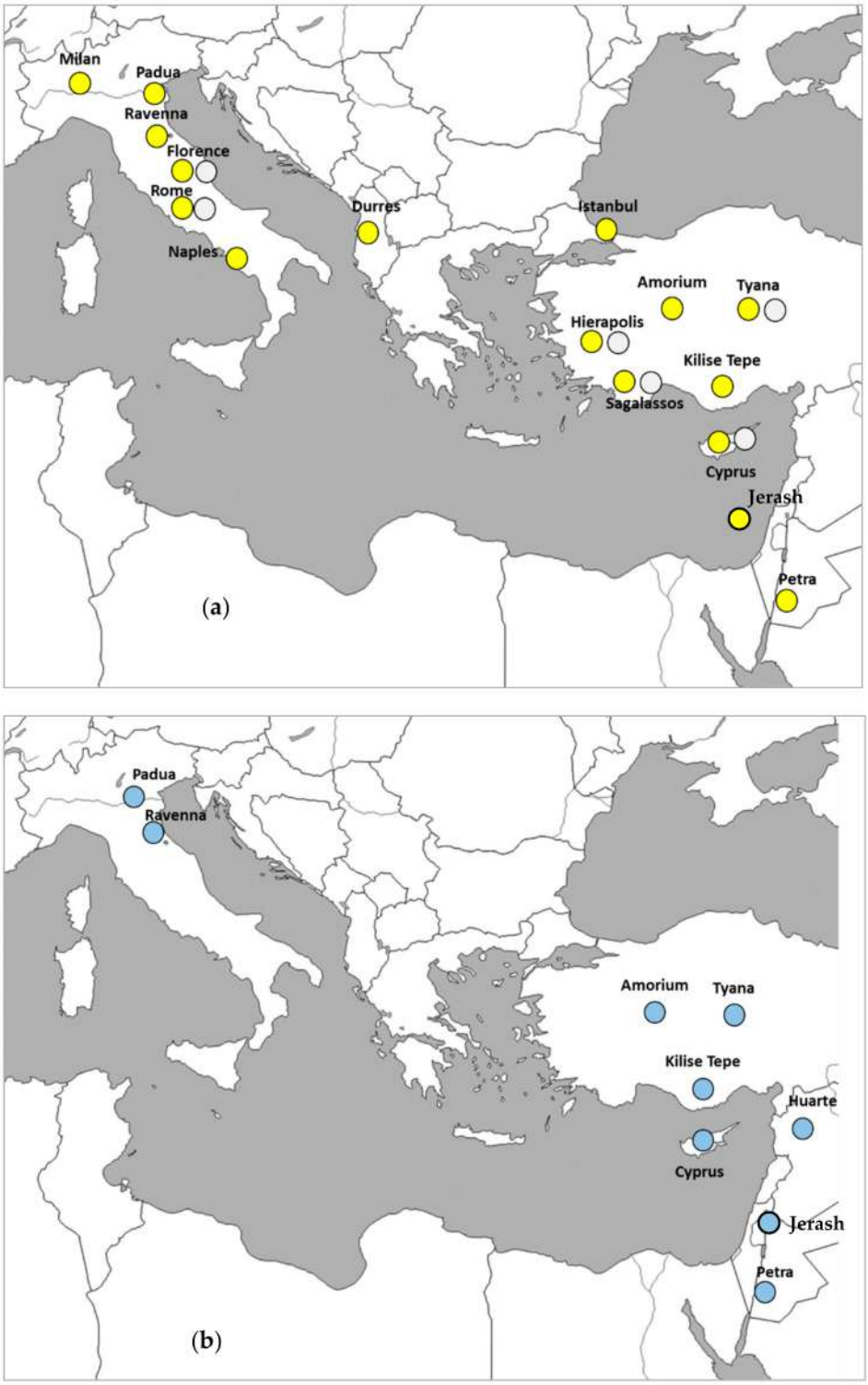

Figure 14. Maps with the indication of sites where tesserae containing (**a**) Sn-based and/or Pb-Sn-based phases and (**b**) P-based phases have been detected. References: Jerash, 4–8th century [70]; Kilise Tepe, 5–6th century [43]; Durres, 6–8th century [44]; Istanbul, 6th century [64]; Cyprus, 6th century [38]; Sagalassos, 6th century [89]; Amorium, 10th century [65]; Hierapolis [43]; Huarte, 5th century [67]; Petra, 5–6th century [68,69]; Tyana, 5–6th century [66]; Naples, 4–9th century [90]; Rome, 16th century [91]; Florence, 13–14th century [92]; Ravenna, 5–6th century [57–61]; Padua, 6th century [55,56]; Milan, 5–6th century [93]; Aquileia, 4th century [73].

How can all the data on colourants and opacifiers be interfaced with the base glass and, thus, correlated with information reported in the historical sources, to help in defining a framework for manufacturing technology and supply of mosaic glass tesserae under the Umayyad caliphate?

3.3. Hypotheses for Plausible Manufacture and Supply Models

Data provided evidence of three compositional categories of glass, pointing to several suppliers. Nevertheless, did tesserae travel as finished products or not?

Analyses demonstrated that the same categories of materials have been used for colouring and opacifying both Levantine and Egyptian raw glass (Table S5). At a first glance, this could suggest that secondary workshops specialised in the production of either one or several colours supplied glass from different primary production centres. However, other hypotheses and models need to be evaluated.

EPMA and LAICPMS analyses allowed distinguishing between Apollonia-type, Foy-2, and Egypt I compositional categories of raw glass. The occurrence of a double supply of glass under the Umayyad caliphate, from Egypt and the Levantine coast, has already been demonstrated [34]. However, a significant difference can be noticed if glass vessels are compared to tesserae: the lack of Foy-2 glass in 7–8th century Umayyad vessels, plus a strong decrease in the use of Apollonia-type in the first half of the 8th century. Moreover, regarding the tesserae, distributional maps in Figure 6 show that Apollonia-type and Foy-2 glass were widely attested among assemblages found across the Mediterranean basin, especially between the 5–10th and the 5–8th centuries; in addition, materials used as colourants and opacifiers in late antique glass mosaics are consistent with those detected in the Umayyad tesserae (Figure 14). The outlined scenario favours the hypothesis that Apollonia-type and Foy-2 tesserae used in Umayyad buildings were recovered from dismantled sites, previously adorned with mosaics. Cited literary sources further strengthen this theory: al-Maqdisī, al-Ya'qūbī, ibn Zabāla, al-Dinawārī, and ibn Rusta reported *mosaic cubes* sent from the Byzantine emperor to Umayyad caliphs, and al-Tabarī also stated that the emperor ordered searches for these *cubes* in ruined cities. It should also be stated that the upsurge of the Umayyad caliphate occurred in the timeframe when the manufacture of mosaics seems to have experienced its major decreases in the Mediterranean basin: between the 7th and 8th centuries, when the number of new buildings adorned with mosaics drastically dropped from more than 50 to first 20 and then 9 exemplars [94]. It is plausible that this decline in mosaic manufacture resulted in a decrease in the demand for tesserae to be produced and, therefore, the use of recovered materials from existing, abandoned monuments, was encouraged.

The occurrence of early Islamic Egypt I glass in the assemblages under study supports the existence of legacies other than Levantine in the manufacture of Umayyad mosaics, attesting the veracity of sources mentioning skilled workmen and materials sent from Egypt [2,11,15,95]. Among materials from Egypt, were tesserae imported as finished product? The fact that the base glasses split into well-known compositional categories suggests there was no mixing of types. Since the mixing is likely to have occurred at secondary workshops if they had worked with different types of raw glass, the hypothesis of ready-made tesserae imported from Egypt, also made by [46], is plausible. However, another possibility is that raw glass travelled with craftsmen, who turned it into coloured tesserae locally, based on known recipes and by using materials available on site. Not only things, but also skills and technological knowledge may have travelled. For the Great Mosque of Damascus and the Dome of the Rock, movements of skilled artisans from Egypt have been attested by historical sources and analyses confirmed that these workmen brought materials with them as well. It is undisputable that adequate storage space for glass and tesserae would have been necessary on site, as well as room for furnaces; however, all these facilities could have easily been available, as the mosaic decorations were made at the same time when the buildings were constructed and, thus, there was a real construction site in progress. The hypothesis of a real transfer of technological

knowledge among craftspeople is also reflected in the context of the Umayyad Caliphate of Spain. Archaeometric analyses carried out on 10th century glass tesserae from the Great Umayyad Mosque of Córdoba (Spain) have provided evidence for Byzantine high-boron glass outside the Byzantine Empire, supporting the theory that tesserae and skilled workmen travelled across the entire Mediterranean [96]. That unfinished tesserae travelled with skilled workmen as raw glass to be coloured and manufactured on site is, therefore, a hypothesis that cannot be excluded, as well as the theory that glass might have been dispatched as cakes to be worked with and cut into small cubes on the construction site.

4. Conclusions

This research demonstrates how, through the comparison between archaeometric data and literary sources, a scenario on glass tesserae manufacture and supply under the Umayyad caliphate (661–750 AD) can be outlined, leading to the emergence of a tale of two legacies.

On the one hand, having found both Apollonia-type and Foy-2 base glasses points to a continuity with the manufacture of mosaic glass tesserae in the late antique Levant. On the other hand, the occurrence of Egypt I glass clearly distinguishes Umayyad tesserae, providing a tangible proof of legacies other than the Byzantine one. This shows that Egypt definitively played a role in the manufacture of mosaics during the Umayyad caliphate, acting as a supplier of not only artisans, but materials as well. Here, at least two possibilities have to be considered: tesserae could have been imported from Egypt as a finished product, ready to be used on site, or could have travelled as raw glass. Which of the two hypotheses might be more consistent, we are currently unable to say; however, this opens the way to a more general remark that will hopefully encourage further debate. The current lack of archaeological evidence to validate any possible model of manufacturing tesserae cannot be ignored. On the one hand, it could be argued that, until sound archaeological evidence has been found, all hypotheses have equal reliability; on the other hand, not having found clear archaeological evidence to support a specific production model could be a result in itself. There probably was not a unique model of production and manufacturing for mosaic glass tesserae, but there were highly skilled artisans that travelled, custodians of a technical knowledge based on the use of specific materials and firing processes. After all, the history of glass has proven that the technology behind colouring and opacifying of this material was encoded in recipes handed down in a real transmission of knowledge. This is known as a result of the Tell-Umar tablet (Iraq, 1400-1200 BC), reporting a recipe for making red glass "*written in a slightly obscure style so as to be understood only by skilled craftsmen*" (*https://www.britishmuseum.org/collection/object/W_1929-0715-1, accessed on 15 July 2021)*.

Supplementary Materials: The following are available online at https://www.mdpi.com/article/10.3390/heritage4040158/s1. Table S1: Tesserae from the qasr of Khirbat al-Mafjar, the Great Mosque of Damascus and the Dome of the Rock selected for this study. Note: when, for opaque tesserae, L* a* b* coordinates are missing, this is due to the irregular surface (or too small size) of the tesserae (and the unfeasibility of VIS-RS measurements). Table S2: Chemical compositions of the glassy matrices of the tesserae, measured with EMPA. All data are expressed as percentage concentrations of element oxides (wt%); n.d. is for not detected. Table S3: Trace element data obtained by LA-ICP-MS, reported in ppm. Table S4: EPMA data acquired on glass standard Smithsonian A during the analyses in comparison with certified data from the literature. Table S5: Summary of data on base glass and colourants/decolourants acquired on all translucent and transparent tesserae from this study.

Funding: This research received no external funding.

Institutional Review Board Statement: Not applicable.

Informed Consent Statement: Not applicable.

Data Availability Statement: The datasets are available from the author on reasonable request. Analysed samples are stored at the Department of Cultural Heritage, University of Bologna-Ravenna campus, within the Conservation Science Laboratory.

Acknowledgments: This paper is based on the research activity carried out by the author as a PhD student at the Department of Cultural Heritage of the University of Bologna. The author owes a huge debt of gratitude to Mariangela Vandini (University of Bologna, Department of Cultural Heritage), for having accurately and patiently supervised her during the Ian Freestone and Liz James are warmly thanked for their support as PhD's thesis external reviewers. The author is sincerely grateful to the anonymous reviewers for their comments and valuable suggestions, which contributed to increase the quality of the manuscript.

Conflicts of Interest: The author declares no conflict of interest.

References

1. Gibb, H.A.R. Arab-Byzantine relations under the Umayyad caliphate. *Dumbart. Oaks Pap.* **1958**, *12*, 219–233. [CrossRef]
2. Gautier-van Berchem, M. The mosaics of the Dome of the Rock in Jerusalem and of the Great Mosque in Damascus. In *Earyl Muslim Architecture*; Creswell, K.A.C., Ed.; Claredon Press: Oxford, UK, 1969; Volume 1, pp. 211–327.
3. Cutler, A. Gifts and Gift Exchange as Aspects of the Byzantine, Arab, and Related Economies. *Dumbart. Oaks Pap.* **2001**, *55*, 247–278. [CrossRef]
4. James, J. Byzantine glass mosaic tesserae: Some material considerations. *Byz. Mod. Greek Stud.* **2006**, *30*, 29–47. [CrossRef]
5. Creswell, K.A.C. *Early Muslim Architecture*, 1st ed.; Claredon Press: Oxford, UK, 1932.
6. Sauvaget, J. *La Mosquée Omeyyade de Médine*; VANOEST: Paris, France, 1974.
7. Hillenbrand, R. *Islamic Art and Architecture*; Thames and Hudson: London, UK, 1999.
8. Rosen-Ayalon, M. *The Early Islamic Monument of al-Haram al-Sharif: An Iconographic Study (Qedem 28)*; Hebrew University, Institute of Archaeology: Jerusalem, Israel, 1989.
9. Allan, J.W. *A Short Account on Early Muslim Architecture*; Revised Edition; Aldershot: London, UK, 1989.
10. Stern, H. Notes sur les mosaïques du Dôme du Rocher et de la Mosquér de Damas. *Cah. Archeol.* **1972**, *22*, 201–217.
11. McKenzie, J. *The Architecture of Alexandria and Egypt: 300 BC—AD 700*; Yale University Press: New Haven, CT, USA, 2007.
12. Bell, H. *Greek Papyri in the British Museum IV The Aphrodito Papyri*; The British Museum: London, UK, 1910.
13. Bell, H. Translation of the Greek Aphrodito Papyri. *Der Islam* **1911**, *2*, 269–283. [CrossRef]
14. Creswell, K.A.C. *Early Muslim Architecture*, 2nd ed.; Claredon Press: Oxford, UK, 1969.
15. McKenzie, J. Alexandria on the Barada. The Mosaics of the Great Mosque in Damascus. In *New Light on Old Glass: Recent Research on Byzantine Mosaics and Glass*; Entwistle, C., James, L., Eds.; The British Museum Press: London, UK, 2013; pp. 291–309.
16. van Lohuizen-Mulder, M. The mosaics in the Great Mosque in Damascus: A Vision of Beauty. *BA Besch* **1995**, *70*, 193–213.
17. Fiorentino, S.; Vandini, M.; Chinni, T.; Caccia, M.; Martini, M.; Galli, A. Colourants and opacifiers of mosaic glass tesserae from Khirbet al-Mafjar (Jericho, Palestine): Addressing technological issues by a multi-analytical approach and evaluating the potentialities of thermoluminescence and optically stimulated luminescence da. *Archaeol. Anthropol. Sci.* **2019**, *11*, 337–359. [CrossRef]
18. Fiorentino, S.; Chinni, T.; Cirelli, E.; Arletti, R.; Conte, S.; Vandini, M. Considering the effects of the Byzantine–Islamic transition: Umayyad glass tesserae and vessels from the qasr of Khirbet al-Mafjar (Jericho, Palestine). *Archaeol. Anthropol. Sci.* **2018**, *10*, 223–245. [CrossRef]
19. Whitcomb, D. *Jericho Mafjar Project*; Annual Report for the Oriental Institute: Chicago, IL, USA, 2013.
20. de Lorey, E. Les Mosaïques de la Mosquéè des Omeyyades à Damas. *Syria* **1931**, *12*, 326–349. [CrossRef]
21. Johnston-Feller, R. *Color Science in the Examination of Museum Objects: Nondestructive Procedures*; The Getty Conservation Institute: Los Angeles, CA, USA, 2001.
22. Jarosewich, E. Smithsonian microbeam standards. *J. Res. NIST* **2002**, *107*, 681–685. [CrossRef]
23. Pouchou, J.; Pichoir, F. Determination of mass absorption coefficients for soft X-rays by use of the electron microprobe. In Proceedings of the 23rd Annual Conference of the Microbeam Analysis Society, Milwaukee, WI, USA, 8–12 August 1988; Newbury, D.E., Ed.; San Francisco Press: San Francisco, CA, USA, 1988; pp. 319–324.
24. Brill, R.H. *Chemical Analyses of Early Glass*; Corning Museum of Glass: New York, NY, USA, 1999.
25. Pearce, J.G.; Perkins, W.T.; Westagate, J.A.; Gorton, M.P.; Jackson, S.E.; Neal, C.R.; Chenery, S.P. A compilation of new and published major and trace element data for NIST SRM 610 and NIST SRM 612 glass reference materials. *Geostand. Newsl.* **1997**, *21*, 115–144. [CrossRef]
26. Longerich, H.P.; Jackson, S.E.; Gunther, D. Inter-laboratory note. Laser ablation inductively coupled plasma mass spectrometric transient signal data acquisition and analyte concentration calculation. *J. Anal. At. Spectrom.* **1996**, *11*, 899–904. [CrossRef]
27. Kamber, B.S.; Greig, A.; Collerson, K.D. A new estimate for the composition of weathered young upper continental crust from alluvial sediments, Queensland, Australia. *Geochim. Cosmochim. Acta* **2005**, *69*, 1041–1058. [CrossRef]
28. Lyliquist, C.; Brill, R. *Studies in Early Egyptian Glass*; Metropolitan Museum of Art: New York, NY, USA, 1993.

29. Paynter, S. Experiments in the Reconstruction of Roman Wood-Fired Glassworking Furnaces: Waste Products and Their Formation Processes. *J. Glass Stud.* **2008**, *50*, 271–290.
30. Henderson, J.; McLoughlin, S.D.; McPhail, D.S. Radical changes in Islamic glass technology: Evidence for conservatism and experimentation with new glass recipes from early and middle Islamic Raqqa, Syria. *Archaeometry* **2004**, *46*, 439–468. [CrossRef]
31. Andreescu-Treadgold, I.; Henderson, J.; Roe, M. Glass from the Mosaics on the West Wall of Torcello's Basilica. *Arte Mediev.* **2002**, *5*, 87–141.
32. Freestone, I.; Jackson-tal, R.; Tal, O. Raw Glass and the Production of Glass Vessels at Late Byzantine Apollonia-Arsuf, Israel. *J. Glass Stud.* **2008**, *50*, 67–80.
33. Tal, O.; Jackson-Tal, R.; Freestone, I. New Evidence of the Production of Raw Glass at Late Byzantine Apollonia-Asurf, Israel. *J. Glass Stud.* **2004**, *46*, 51–66.
34. Phelps, M.; Freestone, I.; Gorin-Rosen, Y.; Gratuze, B. Natron glass production and supply in the late antique and early medieval Near East: The effect of the Byzantine-Islamic transition. *J. Archaeol. Sci.* **2016**, *75*, 57–71. [CrossRef]
35. Brill, R.H. Scientifc investigations of the Jalame glass and related finds. In *Excavations at Jalame, Site of a Glass Factory in Late Roman Palestine*; Weinberg, G.D., Ed.; University of Missouri Press: Columbia, MO, USA, 1988; pp. 257–293.
36. Gratuze, B.; Barrandon, J. Islamic glass weights and stamps: Analysis using nuclear techniques. *Archaeometry* **1990**, *32*, 155–162. [CrossRef]
37. Foy, D.; Picon, M.; Vichy, M. Verres omeyyades et abbasides d'origine egyptienne. In Proceedings of the Annales du 15e Congrès de l'Association Internationale pour l'Histoire du Verre (New York-Corning 2001), Corning, NY, USA, 15–20 October 2001; Association International pour l'Histoire du Verre: Nottingham, UK, 2003; pp. 138–143.
38. Bonnerot, O.; Ceglia, A.; Michaelides, D. Technology and materials of Early Christian Cypriot wall mosaics. *J. Archaeol. Sci. Rep.* **2016**, *7*, 649–661. [CrossRef]
39. Schibille, N.; Gratuze, B.; Ollivier, E.; Blondeau, É. Chronology of early Islamic glass compositions from Egypt. *J. Archaeol. Sci.* **2019**, *104*, 10–18. [CrossRef]
40. Picon, M.; Thirion-merle, V.; Vichy, M. Les verres au natron et les verres aux cendres du Wadi Natrun (Egypte). *Bull. l'Association Française pour l'Archéologie du Verre* **2008**, *22*, 36–41.
41. Foy, D.; Picon, M.; Vichy, M.; Thirion-Merle, V. Caracterisation des Verres de la Fin de L'antiquite En Mediterranee Occidentale: L'emergence De Nouveaux Courants Commerciaux. In *Echanges et Commerce du Verre dans le Monde Antique: Actes du Colloque de l'Association Française Pour L'archéologie du verre Aix-en-Provence et Marseille 7–9 Juin 2001*; Nenna, M.-D., Ed.; Moniqdue Mergoil: Montagnac, France, 2003; pp. 41–85.
42. Conte, S.; Chinni, T.; Arletti, R.; Vandini, M. Butrint (Albania) between eastern and western Mediterranean glass production: EMPA and LA-ICP-MS of late antique and early medieval finds. *J. Archaeol. Sci.* **2014**, *49*, 6–20. [CrossRef]
43. Neri, E.; Jackson, M.; O'Hea, M.; Gregory, T.; Blet-Lemarquand, M.; Schibille, N. Analyses of glass tesserae from Kilise Tepe: New insights into an early Byzantine production technology. *J. Archaeol. Sci. Rep.* **2017**, *11*, 600–612. [CrossRef]
44. Neri, E.; Gratuze, B.; Schibille, N. Dating the mosaics of the Durres amphiteatre through interdisciplinary analysis. *J. Cult. Herit.* **2017**, *28*, 27–36. [CrossRef]
45. Verità, M.; Santopadre, P.; De Palma, G. Scientific investigation of glass mosaic tesserae from the 8th century AD archaeological site of Qusayr' Amra (Jordan). *Boll. ICR* **2017**, *32*, 7–18.
46. Adlington, L.W.; Ritter, M.; Schibille, N. Production and provenance of architectural glass from the Umayyad period. *PLoS ONE* **2020**, *15*, e0239732. [CrossRef] [PubMed]
47. Nenna, M.-D. Egyptian glass abroad: HIMT glass and its markets. In *Neighbours and Successors of Rome: Traditions of Glass Production and Use in Europe and the Middle East in the Later 1st Millennium AD*; Jackson, C., Keller, D., Price, J., Eds.; Oxbow Books: Oxford, UK, 2014; pp. 177–193.
48. Nenna, M.-D. Primary glass workshops in Graeco-Roman Egypt: Preliminary report on the excavations of the site of Beni Salama, Wadi Natrun (2003, 2005–2009). In *Glass of the Roman World*; Bayley, J., Freestone, I., Jackson, C., Eds.; Oxbow Books: Oxford, UK, 2015; pp. 1–22.
49. Kato, N.; Nakai, I.; Shindo, Y. Change in chemical composition of early Islamic glass excavated in Raya, Sinai Peninsula, Egypt: On-site analyses using a portable X-ray fluorescence spectrometer. *J. Archaeol. Sci.* **2009**, *36*, 1698–1707. [CrossRef]
50. Ceglia, A.; Cosyns, P.; Nys, K.; Terryn, H.; Thienpont, H.; Meulebroeck, W. Late antique glass distribution and consumption in Cyprus: A chemical study. *J. Archeol. Sci.* **2015**, *61*, 213–222. [CrossRef]
51. Wedepohl, K.; Simon, K.; Kronz, A. Data on 61 chemical elements for the characterization of three major glass compositions in late antiquity and the middle ages. *Archaeometry* **2011**, *53*, 81–102. [CrossRef]
52. Freestone, I.; Leslie, K.; Thirlwall, M.; Gorin-Rosen, Y. Strontium isotopes in the investigation of early glass production: Byzantine and early islamic glass from the near East. *Archaeometry* **2003**, *45*, 19–32. [CrossRef]
53. Freestone, I.; Gorin-Rosen, Y.; Hughes, M. Primary glass from Israel and the production of glass in Late Antiquity and the Early Islamic period. In *Proceedings of the La Route du verre. Ateliers Primaires et Secondaires du Second Millénaire av. J.-C. au Moyen Age. Actes du Colloque Organisé en 1989 par l'Association Française pour l'Archéologie du Verre (AFAV)*; Nenna, M.-D., Ed.; La Maison de l'Orient et de la Méditerranéen: Lyon, France, 2000; pp. 65–83.
54. Barfod, G.H.; Freestone, I.C.; Lichtenberger, A.; Raja, R.; Schwarzer, H. Geochemistry of Byzantine and Early Islamic glass from Jerash, Jordan: Typology, recycling, and provenance. *Geoarchaeology* **2018**, *33*, 623–640. [CrossRef]

55. Silvestri, A.; Tonietto, S.; Molin, G.; Guerriero, P. The palaeo-Christian glass mosaic of St. Prosdocimus (Padova, Italy): Archaeometric characterisation of tesserae with antimony- or phosphorus-based opacifiers. *J. Archaeol. Sci.* **2012**, *39*, 2177–2190. [CrossRef]
56. Silvestri, A.; Tonietto, S.; Molin, G.; Guerriero, P. The palaeo-Christian glass mosaic of St. Prosdocimus (Padova, Italy): Archaeometric characterisation of tesserae with copper- or tin-based opacifiers. *J. Archaeol. Sci.* **2014**, *42*, 51–67. [CrossRef]
57. Fiorentino, S.; Chinni, T.; Vandini, M. Ravenna, its mosaics and the contribution of archaeometry. A systematic reassessment on literature data related to glass tesserae and new considerations. *J. Cult. Herit.* **2020**, *46*, 335–349. [CrossRef]
58. Fiori, C. Vetro musivo del VI secolo dagli scavi della Basilica di San Severo a Classe (Ravenna). *Riv. Stn. Sper. Vetro* **2011**, *1*, 22–34.
59. Fiori, C. Mosaic Tesserae from the Basilica of San Severo and Glass Production in Classe, Ravenna, Italy. In *New Light on Old Glass: Recent Research on Byzantine Mosaics and Glass*; Entwistle, C., James, L., Eds.; The British Museum: London, UK, 2013; pp. 33–41.
60. Fiori, C.; Vandini, M.; Mazzotti, V. *I Colori del vetro Antico. Il vetro Musivo Bizantino*; Il Prato: Saonara, Italy, 2004.
61. Vandini, M.; Arletti, R.; Cirelli, E. Five Centuries of Mosaic Glass at Saint Severus (Classe, Ravenna). *OCNUS* **2014**, *22*, 91–108.
62. Verità, M. Tessere vitree del battistero Neoniano: Tecniche e provenienza. In *Il Battistero Neoniano. Uno Sguardo Attraverso il Restauro*; Muscolino, C., Ranaldi, A., Tedeschi, C., Eds.; Angelo Longo Editore: Ravenna, Italy, 2011; pp. 73–87.
63. Verità, M. Indagini analitiche delle tessere vitree a foglia d'oro e d'argento dai mosaici teodoriciani e agnelliani di Sant'Apollinare Nuovo. In *Sant'Apollinare Nuovo: Un Cantiere Esemplare*; Muscolino, C., Ed.; Angelo Longo Editore: Ravenna, Italy, 2012; pp. 128–134.
64. Schibille, N.; McKenzie, J. Glass tesserae from Hagios Polyeuktos, Costantinopole: Their early Bizantine affiliations. In *Neighbours and Successors of Rome*; Keller, D., Price, J., Jackson, C., Eds.; Oxbow Books: Oxford, UK, 2014; pp. 114–127.
65. Wypyski, M.T. Technical Analysis of Glass Mosaic Tesserae from Amorium.pdf. *Dumbart. Oaks Pap.* **2005**, *59*, 183–192. [CrossRef]
66. Serra, C.; Silvestri, A.; Molin, G. Archaeometric characterization of vitreous mosaic from Tyana (Cappadocia). In Proceedings of the Late Antique/Early Byzantine Glass in the Eastern Mediterranean. Colloquia Anatolica et Aegaea—Acta Congressus Communis Omnium Gentium Smyrnae II, Izmir, Turkey, 16–17 May 2009; pp. 171–183.
67. Lahanier, C. Etudes des tesselles de mosaïques et de verre à vitre syriens. In *Huarte, Sanctuaire Chrétien d'Apamène (IVe-VIe s.)*; Canivet, M., Canivet, P., Eds.; Institut Français d'Archéologie au Proche-Orient: Paris, France, 1987; pp. 331–346.
68. Marii, F. Glass Tesserae from the Petra Church. In *New Light on Old Glass: Recent Research on Byzantine Mosaics and Glass*; Entwistle, C., James, L., Eds.; The British Museum: London, UK, 2013; pp. 11–24.
69. Marii, F.; Rehren, T. Archaeological coloured glass cakes and tesserae from the Petra Church. In *Annales du 17e Congres del'Association Internationale pour l'Histoire du Verre*; Janssens, K., Ed.; University Press Antwerp: Brussels, Belgium, 2009; pp. 295–300.
70. Boschetti, C.; Lichtenberger, A.; Raja, R.; Wootton, W.; Schibille, N. Loose glass tesserae and lost decorations: Chronology and production of mosaics from Gerasa's Northwest Quarter. *Archaeometry* **2021**, *63*, 960–974. [CrossRef]
71. Vandini, M.; Fiorentino, S. From crystals to color: A compendium of multi-analytical data on mineralogical phases in opaque colored glass mosaic tesserae. *Minerals* **2020**, *10*, 609. [CrossRef]
72. Fiorentino, S.; Chinni, T.; Vandini, M. Materials Inspiring Methodology: Reflecting on the Potential of Transdisciplinary Approaches to the Study of Archaeological Glass. *Appl. Sci.* **2021**, *11*, 8049. [CrossRef]
73. Maltoni, S.; Silvestri, A. A mosaic of colors: Investigating production technologies of roman glass tesserae from Northeastern Italy. *Minerals* **2018**, *8*, 255. [CrossRef]
74. Boschetti, C.; Henderson, J.; Evans, J.; Leonelli, C. Mosaic tesserae from Italy and the production of Mediterranean coloured glass (4rd century BCE–4th century CE). Part I: Chemical composition and technology. *J. Archaeol. Sci. Rep.* **2016**, *7*, 303–311. [CrossRef]
75. Freestone, I.; Stapleton, C.; Rigby, V. The production of red glass and enamel in the Late Iron Age, Roman and Byzantine periods. In *Through a Glass Brightly—Studies in Byzantine and Medieval Art and Archaeology Presented to David Buckton*; Entwistle, C., Ed.; Oxbow Books: Oxford, UK, 2003; pp. 142–154.
76. Arletti, R.; Dalconi, M.C.; Quartieri, S.; Triscari, M.; Vezzalini, G. Roman coloured and opaque glass: A chemical and spectroscopic study. *Appl. Phys. A Mater. Sci. Process.* **2006**, *83*, 239–245. [CrossRef]
77. Maltoni, S.; Silvestri, A. Innovation and tradition in the fourth century mosaic of the Casa delle Bestie Ferite in Aquileia, Italy: Archaeometric characterisation of the glass tesserae. *Archaeol. Anthropol. Sci.* **2016**. [CrossRef]
78. Galli, A.; Poldi, G.; Martini, M.; Sibilia, E.; Montanari, C.; Panzeri, L. Study of blue colour in ancient mosaic tesserae by means of thermoluminescence and reflectance measurements. *Appl. Phys. A Mater. Sci. Process.* **2006**, *83*, 675–679. [CrossRef]
79. Galli, A.; Poldi, G.; Martini, M.; Sibilia, E. Thermoluminescence and visible reflectance spectroscopy applied to the study of blue-green mosaic silica-glass tesserae. *Phys. Status Solidi Curr. Top. Solid State Phys.* **2007**, *4*, 950–953. [CrossRef]
80. Silvestri, A.; Nestola, F.; Peruzzo, L. Multi-methodological characterisation of calcium phosphate in late-Antique glass mosaic tesserae. *Microchem. J.* **2016**, *124*, 811–818. [CrossRef]
81. Penel, G.; Cau, E.; Delfosse, C.; Rey, C.; Hardouin, P.; Jeanfils, J.; Delecourt, C.; Lemaitre, J.; Leroy, G. Raman microspectrometry studies of calcified tissues and related biomaterials. *Dent. Med. Probl.* **2003**, *40*, 37–43.
82. Maltoni, S.; Silvestri, A. Investigating a Byzantine technology: Experimental replicas of Ca-phosphate opacified glass. *J. Cult. Herit.* **2019**. [CrossRef]
83. Zhao, H.; Li, Q.; Liu, S.; Gan, F. Characterization of microcrystals in some ancient glass beads from china by means of confocal Raman microspectroscopy. *J. Raman Spectrosc.* **2013**, *44*, 643–649. [CrossRef]

84. Šefců, R.; Chlumská, Š.; Hostašová, A. An investigation of the lead tin yellows type I and II and their use in Bohemian panel paintings from the Gothic period. *Herit. Sci.* **2015**, *3*, 16. [CrossRef]
85. Welter, N.; Schüssler, U.; Kiefer, W. Characterisation of inorganic pigments in ancient glass beads by means of Raman microscpectroscopy, microprobe analysis and X-ray diffractometry. *J. Raman Spectrosc.* **2007**, *38*, 113–121. [CrossRef]
86. Cloutis, E.; Norman, L.; Cuddy, M.; Mann, P. Spectral reflectance (350-2500 nm) properties of historic artists' pigments. II. Red-orange-yellow chromates, jarosites, organics, lead(-tin) oxides, sulphides, nitrites and antimonates. *J. Near Infrared Spectrosc.* **2016**, *24*, 119–140. [CrossRef]
87. Matin, M.; Tite, M.; Watson, O. On the origins of tin-opacified ceramic glazes: New evidence from early Islamic Egypt, the Levant, Mesopotamia, Iran, and Central Asia. *J. Archaeol. Sci.* **2018**, *97*, 42–66. [CrossRef]
88. Tite, M.; Pradell, T.; Shortland, A. Discovery, Production and Use of Tin-Based Opacifiers in Glasses, Enamels and Glazes From the Late Iron Age Onwards: A Reassessment. *Archaeometry* **2008**, *50*, 67–84. [CrossRef]
89. Schibille, N.; Degryse, P.; Corremans, M.; Specht, C. Chemical characterisation of glass mosaic tesserae from sixth-century Sagalassos (south-west Turkey): Chronology and production techniques. *J. Archaeol. Sci.* **2012**, *39*, 1480–1492. [CrossRef]
90. Schibille, N.; Neri, E.; Ebanista, C.; Ammar, M.R.; Bisconti, F. Something old, something new: The late antique mosaics from the catacomb of San Gennaro (Naples). *J. Archaeol. Sci. Rep.* **2018**, *20*, 411–422. [CrossRef]
91. Arletti, R.; Vezzalini, G.; Fiori, C.; Vandini, M. Mosaic glass from St Peter's, Rome: Manufacturing techniques and raw materials employed in late 16th-century Italian opaque glass. *Archaeometry* **2011**, *53*, 364–386. [CrossRef]
92. Arletti, R.; Conte, S.; Vandini, M.; Fiori, C.; Bracci, S.; Bacci, M.; Porcinai, S. Florence baptistery: Chemical and mineralogical investigation of glass mosaic tesserae. *J. Archaeol. Sci.* **2011**, *38*, 79–88. [CrossRef]
93. Neri, E.; Verità, M.; Conventi, A. Glass Mosaic Tesserae from the 5th to the 6th Century Baptistery of San Giovanni alle Fonti, Milan, Italy. In *New Light on Old Glass: Recent Research on Byzantine Mosaics and Glass*; Faulks, S., Ed.; The British Museum: London, UK, 2013; pp. 1–10.
94. James, L.; Soproni, E.; Bjørnholt, E. Mosaics by numbers. Some preliminary evidence from the Leverhulme Databse. In *New Light on Old Glass: Recent Research on Byzantine Mosaics and Glass*; Entwistle, C., James, L., Eds.; The British Museum: London, UK, 2013; pp. 310–328.
95. James, L. *Mosaics in the Medieval World*; Cambridge University Press: Cambridge, UK, 2017.
96. Gómez-Morón, M.A.; Palomar, T.; Alves, L.C.; Ortiz, P.; Vilarigues, M.; Schibille, N. Christian-Muslim contacts across the Mediterranean: Byzantine glass mosaics in the Great Umayyad Mosque of Córdoba (Spain). *J. Archaeol. Sci.* **2021**, *129*. [CrossRef]